

Unraveling superconductivity in free standing Nb₂C MXene studied through magnetic and magneto-transport properties



Submitted By

Rashida Bibi

Registration No: 00000429874

A dissertation submitted to the National University of Sciences and Technology
Islamabad in partial fulfillment of requirements for the degree of

Master of Science

In

Physics

Supervised By

Prof. Dr. Syed Rizwan Hussain

Department of Physics

School of Natural Sciences (SNS)

National University of Sciences and Technology (NUST)

Islamabad, Pakistan

2022-2024

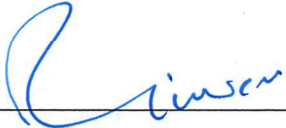
THESIS ACCEPTANCE CERTIFICATE

Certified that final copy of MS thesis written by **Rashida Bibi** (Registration No. **00000429874**), of **School of Natural Sciences** has been vetted by undersigned, found complete in all respects as per NUST statutes/regulations, is free of plagiarism, errors, and mistakes and is accepted as partial fulfillment for award of MS/M.Phil degree. It is further certified that necessary amendments as pointed out by GEC members and external examiner of the scholar have also been incorporated in the said thesis.


Signature: 

Name of Supervisor: Prof. Syed Rizwan Hussain

Date: 23-07-2024

Signature (HoD): 

Date: 23-07-2024

Signature (Dean/Principal): 

Date: 24.7.2024

National University of Sciences & Technology

MS THESIS WORK

We hereby recommend that the dissertation prepared under our supervision by: Rashida Bibi, Regn No. 00000429874 Titled: Unraveling Superconductivity in Free-standing Nb₂C MXene Studied through Magnetic and Magneto-Transport Properties be Accepted in partial fulfillment of the requirements for the award of **MS** degree.

Examination Committee Members

1. Name: DR. FAHEEM AMIN

Signature: (For) 

2. Name: DR. IMRAN HAIDER SAJID

Signature: 

Supervisor's Name PROF. SYED RIZWAN HUSSAIN Signature: 


Head of Department

23-07-2024
Date

COUNTERSIGNED

Date: 24.7.2024


Dean/Principal

Dedicated to my beloved parents

Acknowledgement

Alhamdulillah!

All humbly bow to **Almighty Allah**, who has given me strength and ability to complete my degree, who is the *most Beneficent* and *the most Merciful*. Blessings and Peace be upon the **Holy Prophet Hazrat Muhammad (SAW)**, whose guidance is for the whole humanity. I pay my heartfelt thanks to my loving family especially my **Parents** for their prayers and helping me at every step of my life. I am grateful to my siblings for their belief in me and for making me laugh when it was even hard to smile. My treasured sons, **Abdul Haseeb** and **Musab Farooq** always stayed positive and understanding when my project stole the most precious time of their childhood. I am proud of them. I am also thankful to my husband who rendered his support during my tough times.

I am grateful to the principal of SNS **Prof. Rashid Farooq** for providing a positive research environment.

I am in debt to my supervisor and Head of the Department of Physics **Prof. Syed Rizwan Hussain** for taking an interest in my research field and for giving suggestions to make it more productive. No doubt he is a defining teacher as I learned a lot from the subject he taught. He was always very polite and humble.

I pay my special thanks to my GEC Members **Dr. Faheem Amin** and **Dr. Imran Haider** for their concern and kind guidance. I would like to acknowledge all the faculty and staff of SNS for being so cooperative and friendly. I owe a special thanks to all seniors and fellows for their tremendous efforts to make my research work successful. My Special thanks to **Arooma Syed** who remained very helpful during this project. I am also thankful to **Aruza Naeem** for her moral support that kept me motivated throughout my studies.

I am thankful to *National University of Science and Technology* for giving me a platform for my MS in such a prestigious institute. I spent one of the best academic years in this institute under highly qualified faculty members.

RASHIDA BIBI

Abstract

Magnetism in two-dimensional family is hotspot in today's research due to their promising future technological applications. 2011 redirection the research with the discovery of MXenes with recipe $M_{n+1}X_n$ at Drexel University, Philadelphia. Chemical scissor mediated nanoscale Nb_2CT_x is inherited from parent Nb_2AlC . Superconductivity aspect in wonder material remained under shadow for little period but theoretical prediction soon diverted attention of the world research community and a lot of efforts are being made to fabricate 2-D superconductors and their possible uses in spintronics. The systematic synthesis process at such 2D MXene is described to produce - MXene under optimized conditions using wet chemical etching route. The X-ray diffraction indicates significant increase in c-lattice parameter from 13.92Å to 20.3Å indicating successful etching and intercalation of MXene sheets. Also, c-Lp of Nb_2CT_x free-standing film is further raised from 20.3 Å to 28.24 Å. A typical 2D layered morphology can be seen through SEM images with well-defined lamellar structure. Magnetic measurements of MXene free-standing film unveil the existence of Type-II superconductivity. Magnetization vs. MT curve under field cooled condition indicates a phase transition from normal to superconducting state at $T_c = 90K$ at low temperature with negative magnetization (superconducting diamagnetism) due the formation of vortex state typical of Type-II superconductors. Magneto-transport also reveal the existence of superconductivity by showing a trend toward lower temperature region and large decrease in resistivity. Thus free-standing Nb_2C -MXene film is a type-II superconductor with $T_c=90K$ making a significant development towards superconductivity in 2D materials, thus opening a door towards room temperature attainable Spintronics.

Table of Content

Chapter:1	Introduction.....	1
1.1	Two dimensional materials	1
1.2	Magnetism and superconductivity	2
1.3	Theories of Superconductivity	3
1.3.1	Bardeen- Cooper-Schrieffer (BCS) Theory	3
1.3.2	Meissner effect.....	4
1.3.3	Berezinskii-Kosterlitz-Thouless (BKT) characterization	6
1.3.4	Éliashberg Theory.....	6
1.3.5	Density Functional Theory (DFT).....	7
1.4	Types of superconductors	7
1.4.1	Type-I superconductors / (LTS).....	7
1.4.2	Type-II superconductors / (HTS).....	7
1.5	Types of magnetic materials.....	8
1.5.1	Ferromagnetic.....	8
1.5.2	Antiferromagnetic.....	9
1.5.3	Ferrimagnetic.....	9
1.5.4	Paramagnetic.....	10
1.5.5	Diamagnetic.....	10
1.5.6	Graphical representation.....	11
Chapter: 2	Literature Review	12
2.1	Nanotechnology	12
2.2	MXene from MAX phase	12
2.3	Etching Routes	13
2.3.1	HF Etching	14
2.3.2	Strong acid / Fluoride salt etching.....	15
2.3.3	NH ₄ HF ₂ etching.....	16
2.3.4	Molten salt etching.....	16
2.3.5	Electrochemical etching	17
2.3.6	Chemical vapor deposition (CVD).....	18
2.4	Properties of MXene.....	18

2.4.1	Electronic Properties.....	19
2.4.2	Optical properties.....	19
2.4.3	Mechanical properties.....	20
2.4.4	Magnetic performance	20
2.5	Transport Properties of MAX and MXene.....	20
2.6	Experimental and computational studies on Nb ₂ C MXene.....	22
2.7	Superconductivity in MXenes	23
2.8	Why Niobium (Nb) MXene?.....	24
Chapter 3: Experimental Synthesis and Introduction to Characterizations.....		26
3.1	Synthesis Materials and Tools	26
3.2	Introduction to Characterization Techniques.....	27
3.2.1	X-Ray Diffraction (XRD).....	27
3.2.2	Scanning Electron Microscopy (SEM).....	29
3.3.3	Energy dispersive X-Ray spectroscopy (EDX).....	30
3.3.4	SQUID (Superconducting Quantum Interface Device, MPMS).....	31
3.3.5	Physical Properties Measuring System (PPMS)	32
Chapter: 4 Synthesis and Characterization of Nb ₂ CT _x Free-Standing film.....		33
4.1	Synthesis of Nb ₂ CT _x MXene	33
4.2	Synthesis of Nb ₂ CT _x Free Standing Film.....	33
4.3	Structural and Morphological Analysis.....	34
4.3.1	XRD Analysis	34
4.3.2	SEM & EDX Analysis	35
4.3.3	XPS Studies.....	36
Chapter: 5 Magneto-Transport properties of Nb ₂ CT _x Free-Standing Film		38
5.1	Temperature dependent magnetization	38
5.2	Magneto-transport Properties.....	39
Conclusion		42
Future Perspective		43
References.....		44

List of Figures

Fig 1. 1 Examples of 2D materials ⁷	1
Fig 1. 2 Periodic table of superconductivity ¹⁴	3
Fig 1. 3 Cooper Pair moving inside a crystal lattice ¹⁸	4
Fig 1. 4 Meissner effect ¹⁸	6
Fig 1. 5 Types of superconductors ²²	8
Fig 1. 6 Magnetic domains in ferromagnetic materials ²³	9
Fig 1. 7 Magnetic domains in antiferromagnetic materials ²³	9
Fig 1. 8 Magnetic domains in ferrimagnetic materials ²³	10
Fig 1. 9 Comparison between Paramagnetic and Diamagnetic materials ²⁶	11
Fig 1. 10 Graphical insight of magnetic behaviours.....	11
Fig 2. 1 Early timeline for MXene discovery ³¹	13
Fig 2. 2 Schematics for HF etching ³⁰	
Table 2. 1 Transition Temperature T _c for MXene verified experimentally and calculated through DFT Study	24
.....	14
Fig 2. 3 Schematics for fluoride salt ⁵⁰	15
Fig 2. 4 Schematics of molten salt etching ⁴⁸	17
Fig 2. 5 Schematics for electrochemical etching ⁶¹	18
Fig 3. 1 X-Ray diffraction through crystal lattice ⁹²	28
Fig 3. 2 Schematics and working principle of scanning	
Table 3. 1 Chemicals utilized for etching of Nb ₂ C.....	26
electron microscope ⁹³	29
Fig 3. 3 Working principle of energy dispersive X-Ray spectroscopy ⁹⁴	30
Fig 4. 1 Schematic of synthesis route of Nb ₂ CT _x free-standing film.....	34
Fig 4. 2 (a) XRD spectra of the MAX Nb ₂ AlC, Nb ₂ CT _x MXene and Nb ₂ CT _x MXene Free-standing film	35
Fig 4. 3 SEM images of (a) Nb ₂ AlC MAX phase at 10 μm (b) HF etched Nb ₂ CT _x MXene at 5 μm (c) Delaminated Nb ₂ CT _x MXene at 10 μm (d) Elemental analysis of each element in Nb ₂ CT _x MXene Free-standing film.....	36
Fig 4. 4 . (a) XPS spectra for Nb ₂ CT _x MXene. Deconvolution of high-resolution XPS plot for Nb ₂ CT _x MXene (b) Nb 3d.....	37

Fig 5. 1 ZFC and FC curves at 100 Oe, 500 Oe and 1K Oe for Nb₂C free-standing film 39

Fig 5. 2 (a) Temperature vs Resistivity (left y-axis) and magnetic moment (right Y-axis) at H=0, 41

Chapter:1 Introduction

1.1 Two dimensional materials

A journey that started from stone age successfully entered the era of new materials^{1,2}. The discovery of two-dimensional materials redirected the research with potential of adding new members in the family in just few decades. Many new materials with novel properties are already been introduced, while others are in pipeline and await discovery^{3,4}. These materials exhibit diverse properties ranging from semimetals to metals and insulator to semiconductors⁵. Single atom thick crystals have strikingly different behaviour from their 3D counterpart, e.g. graphene is 2D semiconductor with zero-band gap while graphite is semimetal with overlapped band gap. Similarly, transition metal dichalcogenides TMDCs have band gap semiconductors in 2H phase while bulk form has indirect band gap. A mixture of compounds with varying properties has created multifaceted heterostructures, developing new physical effects and creation of novel devices like Josephson junction, superconducting quantum interference devices (SQUID), superconducting transistor and superconductor-quantum dot hybrid devices⁶. Boron Nitride in hexagonal structure (h-BN), polymers, hydroxides with double layers (LDHs), metal organic frame works (MOFs), bisphenols (BPs) and different metal oxides are famous examples of 2-D materials⁷.

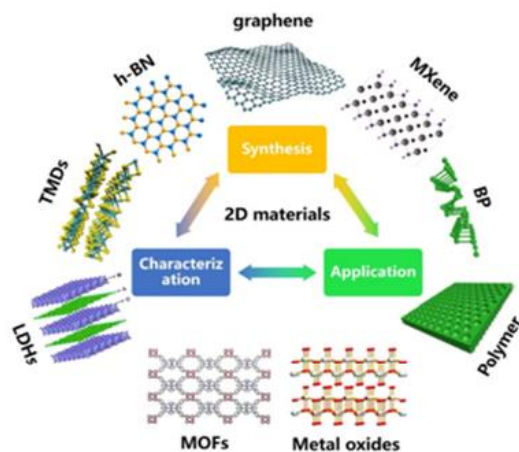


Fig 1. 1Examples of 2D materials⁷

1.2 Magnetism and superconductivity

The history of magnetism dates back to ancient times when lodestones were 1st found to attract the pieces of iron. Loadstone is naturally occurring mineral, Greek named it as “Magnetite” - the Magnesian stone ". Aristotle was the first who generated a scientific discussion about magnetism in his period 625 BC to about 545 BC. Chinese were among the pioneers who used magnetic compass in 12th century for navigation. Human curiosity continued its research to further explore about magnetism for centuries and finally 19th century came up with findings worth mention. Relationship between electricity and magnetism was accidentally established by Hans Christian Orested in 1819 while mathematical relation between both was given by J B Biot and F Savart named as Biot-Savart Law in 1820. Michael Faraday in 1831 found that current induces when time varying magnetic fields are present. James Clerk Maxwell in 1861 unified electricity and magnetism through Maxwell equations. Electromagnetism remained key study area even during 20th century and still a hotspot in 21st century in different dimensions of materials (3D, 2D, 1D)⁸.

Superconductivity⁹⁻¹² is one of the exotic concepts in physics discovered a century ago gets an iron boost¹³ in last few decades. In 1911 Kamerlingh Onnes (Nobel Prize - 1913) and Holst discovered superconductivity in mercury at 4.2 K, -268°C), temperature of liquid helium. Almost after 50 years, in 1957 BCS theory, was developed to explain the physics of this property. In 1986 Bednorz and Müller discovered superconductors behaving so at high temperature called “cuprate- ceramic materials” with higher transition temperatures around 135 K generating a new debate about basics of this phenomena and for applications at room-temperature. After discovery of superconductivity if mercury, a race for discovery of new materials demonstrating superconductivity at cryogenic temperature started but after a lot of efforts to achieve practically viable and economically feasible applications operative at room temperature impeded further progress for 75 years until 1986 when cuprate were discovered at ambient pressure with highest T_c of 135 K by Bednorz and Müller (Nobel Prize – 1987) with only challenge of ceramic nature that makes them brittle¹².

Magnetism and superconductivity are two important properties which are closely interrelated and are explained by BCS theory and Meissner effect. Meissner effect talks about expulsion of magnetic field from inside the superconductor against the normal state where it

“Electron experience a special kind of attraction interaction, overcoming coulomb force of repulsion between them, as a result of cooper pair”.

These pairs experience no scattering i.e. they move without facing any resistance through lattice and material is said to be superconductor. Visualize an e^- surrounded by $+$ ly charged ions with attractive interaction among the e^- and neighboring ions deforming the lattice around the e^- . This appears as a positively charged cloud attracting the second e^- . Lattice vibrations are quantized forming phonons. This pair is macroscopic coherent quantum state with different coherence lengths depending upon lattice structure. “Distance between the paired electrons is called coherence length” which is very large in soft superconductors and exceed 100 nm. This means in these superconductors a good no of cooper pairs co-exists in a unit volume and thus overlap. Energy of this state must be lowered to be favored over the normal state. Energy gain resulting from the pair formation is called the energy gap which can be measured directly and is a good parameter to confirm superconductivity. Electron-lattice-electron interaction is strengthened only if two electrons have equal and opposite spin and momentum¹⁷.

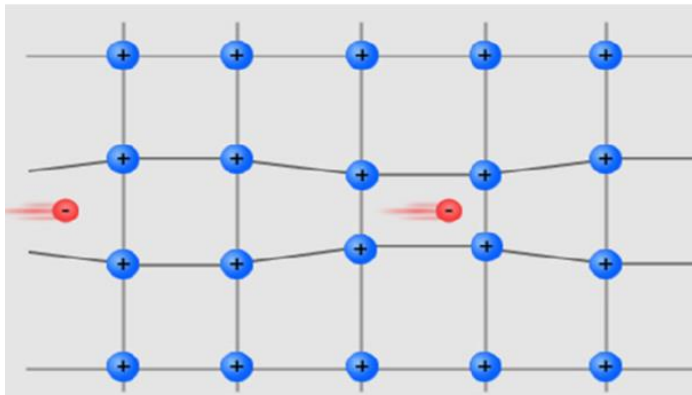


Fig 1. 3 Cooper Pair moving inside a crystal lattice¹⁸

1.3.2 Meissner effect

“Expulsion of magnetic field from a superconductor during its transition to the superconducting state when it is cooled below the critical temperature is called Meissner effect”¹⁹.

Under a situation if superconductor has no magnetic field inside it is said to be in Meissner state and is explained by BCS theory. This state vanishes when the external magnetic field is too strong. Superconductors are classified into two categories according to the critical temperature. “Low Temperature superconductor (LTS)” known as soft, type-I or conventional superconductors. While 2nd class is named as “High temperature superconductor (HTS)”, hard, type-II or unconventional superconductors. Two brothers Fritz and Heinz, commonly known as “London brothers” showed that the EM free energy in a superconductor is least if it follows given equation.

$$\nabla^2 \mathbf{H} = -\lambda^{-2} \mathbf{H}$$

London equation

H - Magnetic field

λ - London penetration depth

This relation implies that the magnetic field decreases exponentially from its initial value it possesses at the surface in a superconductor. Exclusion of magnetic field is exhibition of the super-diamagnetism arises during the process of phase transition from conductor to superconductor by decreasing temperature lower than critical temperature. Perfect diamagnetism is exhibited by Meissner state superconductors, also called as super-diamagnetism that means the magnetic field in total is very close to zero inside the penetration depths as compared to the surface with negative volume magnetic susceptibility. Instantaneous magnetization in a material which opposes the direction of external field make diamagnetic material. The origin of diamagnetism in different materials and superconductors varies. Diamagnetism arises due to the orbital spin of electrons about the nucleus of an atom. This is electromagnetically induced by applying external field in conventional materials while perfect diamagnetic behaviour comes from continuous current flowing opposite to the applied field. Hence Meissner effect is not only due to the orbital spin.

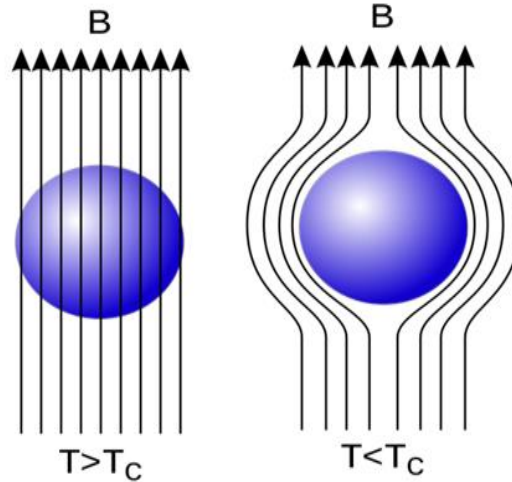


Fig 1. 4 Meissner effect¹⁸

1.3.3 Berezinskii-Kosterlitz-Thouless (BKT) characterization

In statistical physics, bound “vortex and antivortex” pairs at low temperatures experience a shift to unpaired vortices anti-vortices” at critical temperature in 2-D XY model. The concept was suggested by “Vadim Berezinskii, John M. Kosterlitz and David J. Thouless” famously known as (BKT). Such transitions are present in 2-D systems of condensed matter branch of physics which are estimated by this model. Currently this term is also used to the “Cooper pair pinning” in the insulating region²⁰.

1.3.4 Éliashberg Theory

Perturbation approach applied to systems containing many bodies and showing superconductivity is termed as Éliashberg theory. It is a GW approximation applied in the presence of a “superconducting proximity effect” field with screened interaction (W) both Coulomb and phonon propagators. BCS pairing is not considered here rather the interactions are calculated from 1st principles. Hamiltonian (H) is 1 for interacting e^- and ions with decoupled lattice dynamics. Electron–phonon coupling is explained within the “Kohn–Sham theory”. To establish perturbative approach, Hamiltonian is divided in a “zero-approximation H_0 ” plus an “interaction part H_I ”²¹.

1.3.5 Density Functional Theory (DFT)

Most versatile and popular computational “Quantum-mechanical modelling” technique applied in physics to study electronic structure of many body systems like atoms and condensed phases. An extension to this method is superconductors density functional theory (SCDFT) to handle long peculiar symmetries present in superconductors. SCDFT is also helpful in predicting superconductivity in newly emerging materials especially for the investigation of superconductive behaviour under high pressure²¹.

1.4 Types of superconductors

1.4.1 Type-I superconductors / (LTS)

“Materials which losses their superconductivity abruptly when the strength of the applied field rises above a critical value (H_c) named as Type-I superconductors”. These are also called as low temperature super conductors (LTS) and are well explained by Meissner effect. These materials show perfect diamagnetism and are called as soft or conventional superconductors. Aluminum (Al), Mercury (Hg), lead (Pb) belongs to this class of superconductors.

1.4.2 Type-II superconductors / (HTS)

“Materials which carry very large current in the presence of higher magnetic fields and do not show Meissner effect but characterized by the mixed state with intermediate state are classified as Type-II superconductor”. These are also called as High temperature super conductors (HTS) and are explained by different theories depending upon type of material/compound. The magnetic flux and super electrons flow in different regions. At the start of the process magnetic induction is zero in the interior region showing Meissner effect while increasing applied field after H_{c1} takes to a mixed vortex state with distinction of an increased amount of magnetic flux penetrating inside the material²². Superconductivity vanishes at second field H_{c2} that is also critical. Sometimes, type-II superconductors offer resistance in mixed state. This is caused by the movement of the flux vortices induced by the Lorentz forces. Mixed state is generated due to vortices present in the electronic superfluid, known as “fluxons”. Generally

pure elemental superconductors are type I except Nb and carbon nanotubes CNTs while almost all compound and impure superconductors are from the class of type II.

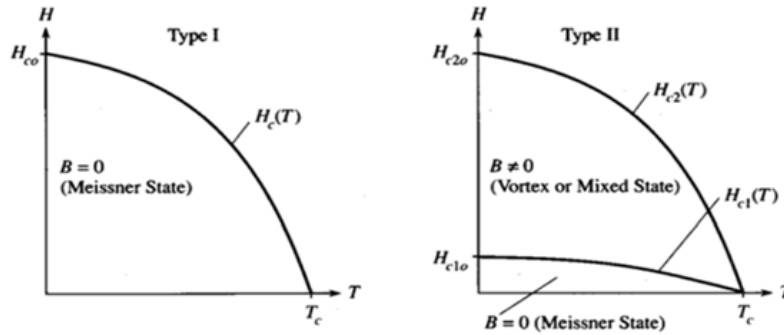


Fig 1. 5 Types of superconductors²²

1.5 Types of magnetic materials

1.5.1 Ferromagnetic

“Substances which are strongly attracted by a magnet” with large positive susceptibility and retain magnetic behaviour even after the removal of external field are named as ferromagnetic materials. Atomic moments in magnetic materials, such as iron, nickel, and magnetite, interact intensely with one another. The atomic moments align in either a parallel or antiparallel orientation are propelled by electronic exchange process giving a larger magnetization even if magnetic field is absent²³. The exchange forces are around 100 million times greater than the Earth's magnetic field, equivalent to a field of about 1000 Tesla. The exchange force arises from the relative spin orientation of two electrons that is quantum mechanical effect. Spontaneous magnetization whose magnitude, at 0K, depends upon spin magnetic moment of electrons and magnetic ordering temperature exist in these substances. Common examples include Co, Fe, Ni and their alloys²⁴.

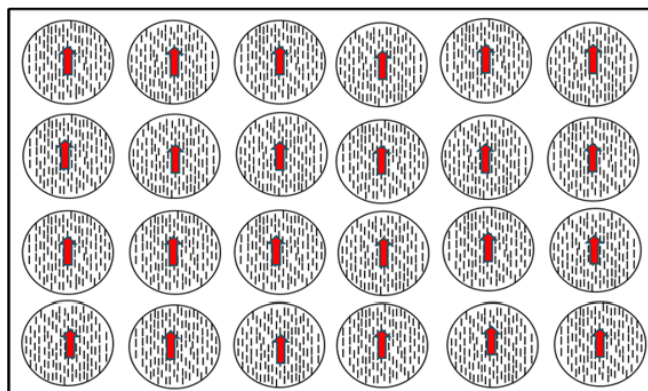


Fig 1. 6 Magnetic domains in ferromagnetic materials²³

1.5.2 Antiferromagnetic

“The materials which possess the magnetic moment aligned in regular pattern with neighboring spins pointing in opposite direction are called as antiferromagnetic” introduced in 1933 by L. Landau. Susceptibility behaviour with critical temperature tagged as Neel temperature T_N depicts the presence of antiferromagnetism. This behaviour is generally found in transition metal compounds and oxides like hematite, chromium, alloys of iron manganese and Nickel oxide etc²⁵.

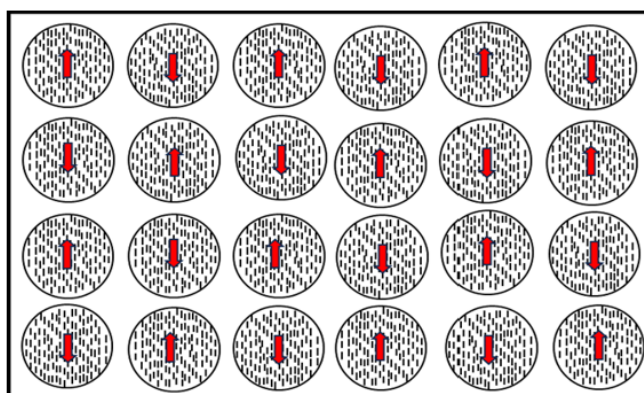


Fig 1. 7 Magnetic domains in antiferromagnetic materials²³

1.5.3 Ferrimagnetic

“Materials in which magnetic moments are present in unequal magnitude and spontaneous magnetization exist are called as ferrimagnetic”. Ionic compounds like oxides have complex forms of magnetic ordering due to crystal structure. Ferrimagnetics and ferromagnetics share similarity of Curie temperatures, hysteresis, spontaneous

magnetization and remanence but only difference of magnetic ordering. Magnetite and yttrium iron garnet are common example.

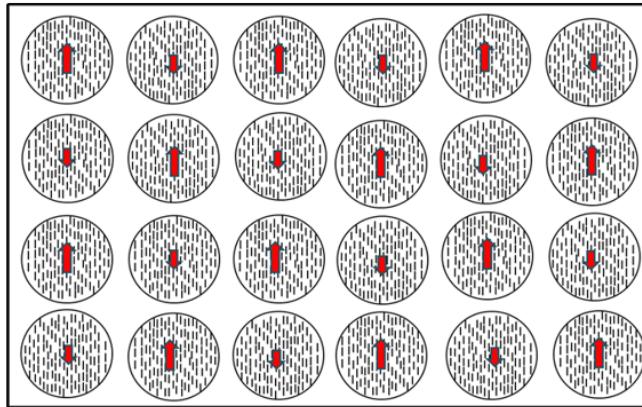


Fig 1. 8 Magnetic domains in ferrimagnetic materials²³

1.5.4 Paramagnetic

Para-magnetism occurs when specific materials produce internal magnetic fields that align, though faintly attracted, with an external magnetic field. Net magnetic moment exists in few atoms or ions due to unpaired electrons in partially filled orbitals. Net magnetization gets zero when external source vanishes. There is partial alignment of magnetic moments in the direction of applied field giving positive magnetization (also positive susceptibility). At moderate field and temperatures, the paramagnetic susceptibility is small (but larger than diamagnetic). Randomizing effects opposes the field efficiency of aligning moments. Biotite, Siderite, Montmorillonite, Pyrite, Nontronite are example of this kind of material.

1.5.5 Diamagnetic

“External magnetic field produces induced magnetic field in its opposite direction causing a repulsive force inside a material resultantly material is expelled by this field representing diamagnetism”. Materials showing zero net magnetic moments due to filled orbitals and no unpaired electrons exhibit this behaviour. On exposure to external magnetic field negative magnetization (or negative susceptibility) is experienced. All materials are fundamentally diamagnetic with reason of non-cooperative behavior of electrons orbiting around. Sometimes weak magnetization exists on exposure to field.

Quartz (SiO_2), Calcite (CaCO_3), H_2O are examples.

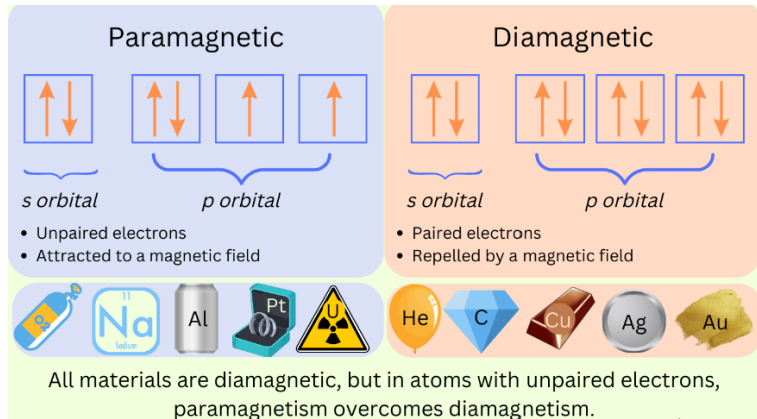


Fig 1. 9 Comparison between Paramagnetic and Diamagnetic materials²⁶

1.5.6 Graphical representation

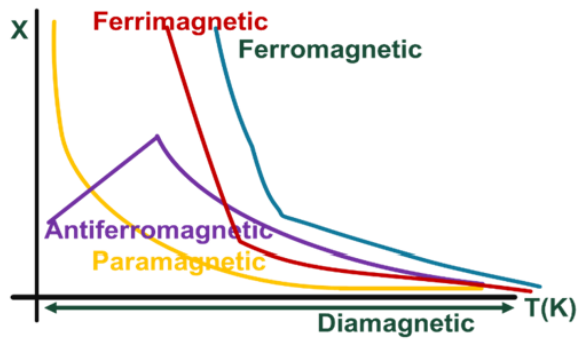


Fig 1. 10 Graphical insight of magnetic behaviours

Chapter: 2 Literature Review

This work primarily focused upon the synthesis of 2D TMCs named “MXenes” and its applications in magnetism and superconductivity. This family of materials possesses promising properties and applications in various fields like energy storage, electronics, biomedical applications, magnetism and electromagnetic shielding.

2.1 Nanotechnology

Few decades ago, science fiction novels used ideas and terms which fascinate the world but it is today’s reality offering glimpse into the magic of tomorrow. Among these fantasies are smart materials using nanotechnology. According to Wikipedia “The manipulation of matter with at least one dimension, sized from 1 to 100 nanometers (nm) is called nanotechnology”²⁷. In 1959 Richard Feynman talked on the topic “There is plenty of room at the bottom” seeding the seed of concept of nano scale technology. One billionth/ 10^{-9} of a meter is called one nanometer (nm). “Carbon–carbon bond” lengths is in the range of 0.12–0.15 nm and DNA double-helix exist with a diameter approximately 2 nm. At nano scale material show novel optical, electrical and magnetic properties in comparison to their bulk counterpart.

2.2 MXene from MAX phase

2011 took a quantum leap in the introduction of novel 2D materials tagged as MXene²⁸ when Michael Naguib and his team at Drexel University, Philadelphia, USA discovered a new 2D material known as “MXene”²⁹. They did it successfully by synthesizing the 2D network of MXene sheets through wet chemical etching route of parent 3D MAX phase³⁰. This discovery opened up new avenues of research for upcoming many years³¹. Transition metal carbides or nitrides with hexagonal panel structure³² with architectural description of $M_{n+1}AX_n$ are classified as MAX where M is from initial transition metals like Cr, Ti, Mo, V, Sc, Zr, Nb and X takes its share from C and/or N, A is element chosen from G-3 or G-4 within the periodic table while “n” varies from 1 to 3. So possible MAX segments are with 413, 312, and 211 arrangements³³. Versatile MXene family has general recipe $M_{n+1}X_nT_x$ in which M stands for early transition metals from group III-VI (like Ti, Mo, V, W, Nb, Ta), X denotes C and/or N. T_x implies surface termination of -O, -OH, -F and -Cl and $n=1-4$ ³. Formula based stoichiometric ratio³⁴ with a particular structure resembling graphene³⁵,

tagged as MXene, gained a widespread acknowledgement owing to their scalability²⁸, ease of processing, hydrophilicity³⁶, favorable optical³⁷, electrical, thermal, electronic³⁸ and mechanical properties³⁹. This diverse material family garnered exceptional attention in research due to electrochemical energy storage⁴⁰, electromagnetic interference shielding, medicine and environmental remediation⁴. Today, it has become imperative for scientific community to safely synthesis MXene from MAX phase using different synthesis routes⁴¹ like alkali extraction, molten salt or halogenation. Following etching, MXene exist in multilayer form (MXene flakes, stacks), powdered form, free standing films, composites, fibers, aerogels or supported films. Intercalants and functional group^{30,36} like -O, -H, -OH, present are used to alter the physical properties in MXene⁴².

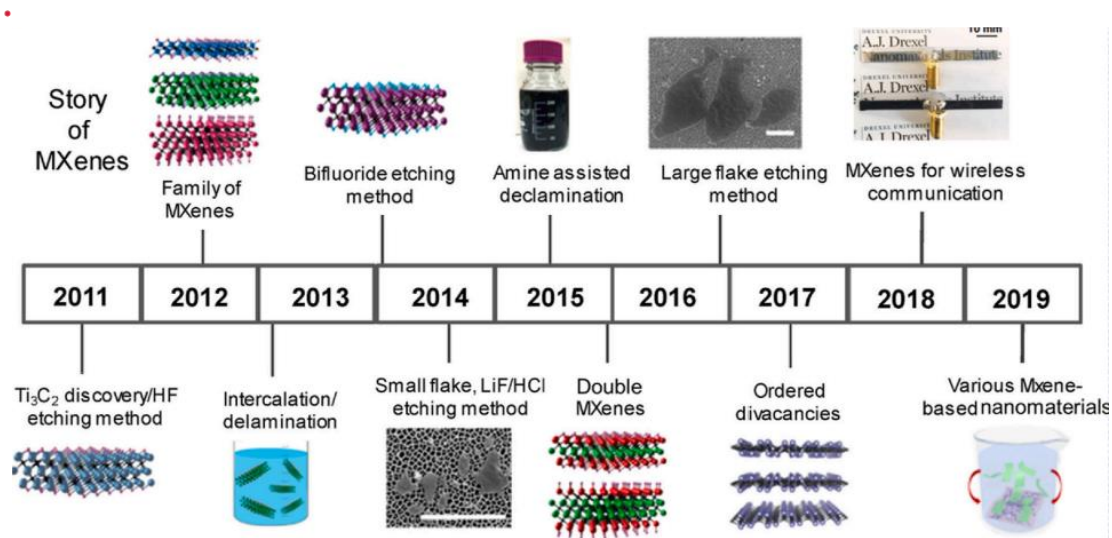


Fig 2. 1 Early timeline for MXene discovery³¹

2.3 Etching Routes

2D layer structured MXene are acquired through the etching of their respective 3D precursor MAX phases where chemical bond between the elements of MAX phase is broken down and then etched out of it⁴³. By nature, MA is metallic bond and MX bond is ionic/covalent/ hybrid character. High temperature cause the breakdown of MA and MX bonds⁴⁴ and after etching with corrosive media like HF or any other acid, M and A are etched out forming derivatives of respective precursors. MAX phases of pattern $M_{n+1} A X_n$, have variable etching conditions due to the influence of n on different MXene and their composites. E.g. $Mo_2Ti_2AlC_3$ (here n = 3) has etching time double of Mo_2TiAlC_2 (with n = 2) keeping similar etching conditions. Wet Chemical

Etching^{36,45}, Chemical vapor deposition⁴⁶, molten salt etching⁴⁷ and electrochemical etching⁴⁷ are different routes in practice to get MXene.

2.3.1 HF Etching

Aluminum (Al) based MXene are preferably etched using HF. Naguib et al. 1st proposed use of HF³⁶ in 2011 in which MAX phase in powder form is immersed into a predetermined concentration of aqueous solution of hydrochloric acid under optimized conditions already established. Solids separated from supernatant are centrifuged or filtered. Mixture is repeatedly washed with deionized water until neutral pH is achieved and resultant MXene powder is obtained after drying. Exfoliation takes place and different layers separate from each other. Following equation explains chemical⁴⁸.



Srivastava et al. carried out exfoliation of Ti₃C₂ from Ti₃AlC₂ via fluoride acid in which F acted as a termination and interlayer spacing was increased allowing further intercalation of HF resulting into AlF₃ and H₂⁴⁹. Main advantage of using HF as etchant is that it maintains lamellar structure making it a good substrate but on the other hand etched MXene can corrode due to strong corrosive nature of acid causing damage to surface of the final product. Furthermore, HF is harmful to human health when exposed for larger time which limits its application as etchant for many applications⁴⁷.

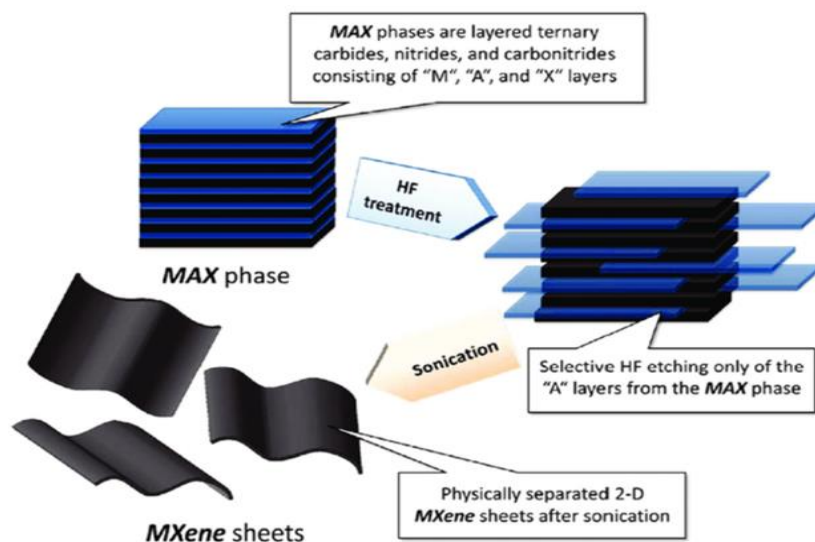


Fig 2. 2 Schematics for HF etching³⁰

2.3.2 Strong acid / Fluoride salt etching

In effort to find alternatives of etching, Michael et al. used an unconventional technique in which MXene was etched from corresponding MAX phase using a solution of LiF and HCL instead of HF in 2014⁵⁰. Result was hydrophilic “clay” like material, more conductive solid once dried and can be rolled into films of minimal thickness. This MXene clay exhibit exceptional rate performance and cyclability giving volumetric capacitance around 900 F/cm³ which can be used as supercapacitors electrode in H₂SO₄ electrolyte⁵¹.

Ghidiu et al. used HCl and fluoride salts⁵¹ in 2015 in order to develop a safe etching route. Ti₃AlC₂ in powder form is gradually mixed with aqueous solution of LiF/HCl that was already prepared on moderate temperature. In 2021, same method is used by Zhu et al.⁵². Here, 20 ml HCL with molarity 9M is mixed with 1.6g of LiF. Then, 1 g of Ti₃Al₂ (powder form) is mixed into the acid mixture with continued stirring in a Teflon bottle for 24 h at 35 °C. Resultant products is repeatedly washed using deionized water to get neutral pH. Sonication resulted in delaminated Ti₃C₂T_x suspension. In this method LiF with mild acidity react with HCl producing HF, instead of direct use of HF improving the safety.

Sodium flouride can also be used as fluoride salt in place of LiF. V₂AlC powder is etched with NaF plus HCl at 90 °C by Liu et al. in 2017 successfully acquired V₂C powder⁵³.

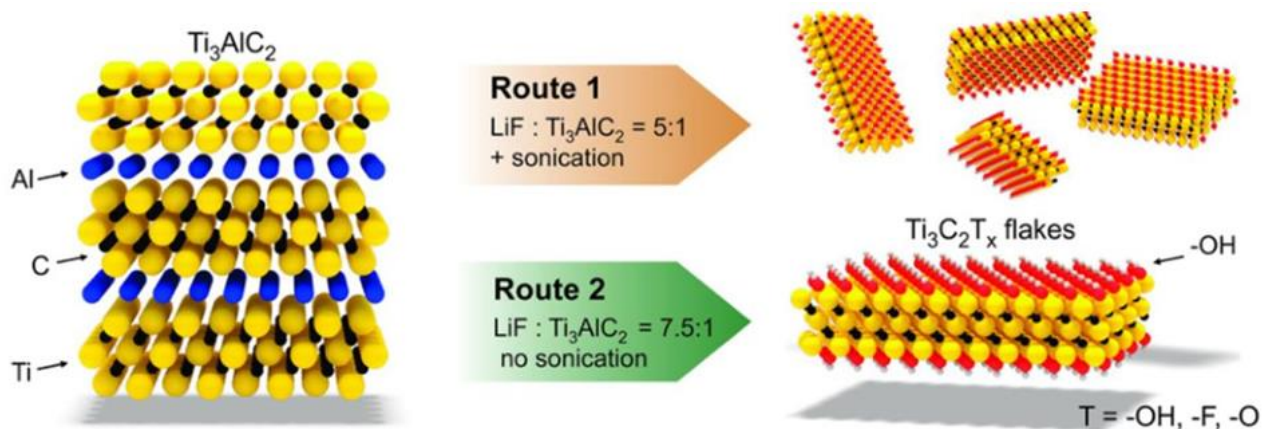


Fig 2. 3 Schematics for fluoride salt⁵⁰

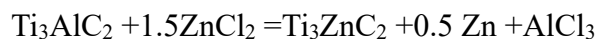
2.3.3 NH₄HF₂ etching

In 2014 and 2019, J. Halim et al. published a method of fabrication of epitaxial thin films by etching the Ti₃AlC₂ in aqueous HF or NH₄HF₂ solution at room temperature⁵⁴ resulting 25% increase in c-parameter (~25Å) when treating with NH₄HF₂ as compared to its value upon treating with HF. Both films exhibit metallic conductivity to 100K temperature. Upon further decrease in temperature, it shows negative trend in its resistivity which increases with decreasing the temperature conferring negative magnetoresistance (MR)⁵⁵.

In 2019 Feng et al. devised the use of NH₄HF₂ for etching of MXene with better interlayer spacing⁵⁶. Here, 1 g Ti₃AlC₂ powder is added in NH₄HF₂ while stirring at 60 °C. Washing is carried out by using deionized water until neutral pH is achieved. Supernatant is centrifuged and dried at 80 °C for 12 h in a vacuum oven giving with higher purity of MXene. NH₄⁺ are used to increase interlayer spacing with better pseudo capacitance and specific capacitance 34% higher than that of Ti₃C₂ etched with HF. Organic polar solvents can be useful to etch and delaminate MXene with NH₄HF₂, explored by Natu et al.⁵⁷ in 2020. NH₄HF₂ decomposed into HF and NH₄F in polar solvents with some residue.

2.3.4 Molten salt etching

Gogotsi et al. are pioneer for developing 1st 2D transition metal nitride-Ti₄N₃T_x MXene⁵⁸ using molten salt to selectively etch out Al from Ti₄AlN₃ MAX phase. Li et al. conducted a series experiments to get MAX phase with zinc by applying “elemental-replacement method” using molten ZnCl₂ and etching resulted the formation of Ti₃C₂Cl₂ and Ti₂CCl₂ MXenes by gradual stripping Ti₃ZnC₂ and Ti₂ZnC⁴⁷. Lewis acid showed a strong acidity such as in ZnCl₂ and this environment help to remove Al from MAX phase. In this method, a mixture of Ti₃AlC₂ and ZnCl₂ is prepared in ratio 1:1.5 as raw material. Path for Zn-containing MAX-phase formation can be explained in a simplified reaction given below⁴⁷.



It is quick etching method at room temperature especially for etching of those MXene which are used for supercapacitor applications. Chemical used here are least harmful proving better health safety.

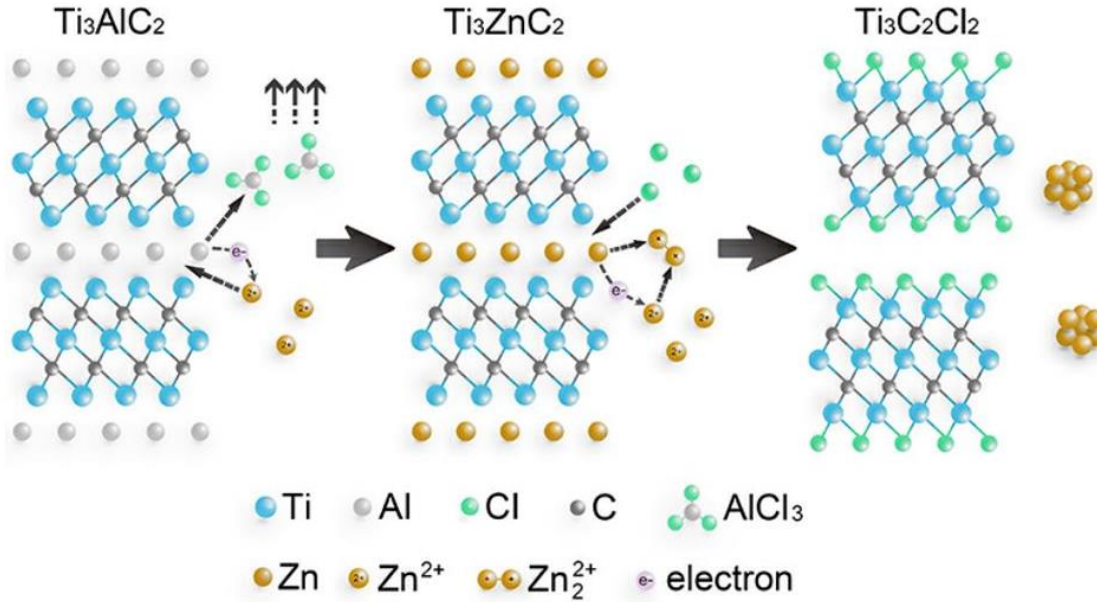
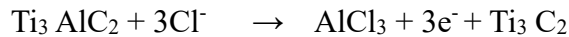


Fig 2. 4 Schematics of molten salt etching⁴⁸

2.3.5 Electrochemical etching

Although etching methods primarily vary with type of etchant used but these etchants can affect the properties of final product⁵⁹. In order to overcome the undesirable results and achieve room temperature etching, electrochemical etching method is prescribed. Yang et al. employed anodic etching method in an aqueous electrolyte on Ti₃AlC₂ MAX phase⁶⁰. An alkaline solution containing NH₄Cl and tetramethylammonium hydroxide (TMA-OH) terminated into Ti₃C₂T_x (T_x =OH, O). Ti₃AlC₂ acted as anode and chloride ion in the electrolyte corrosion Al at anode breaking the Ti-Al bond. Chemistry of whole reaction is as below⁶¹.



No F-terminations were observed in exfoliated Ti₃C₂T_x flakes as no fluorine is used in this method bringing novelty in electrochemistry.

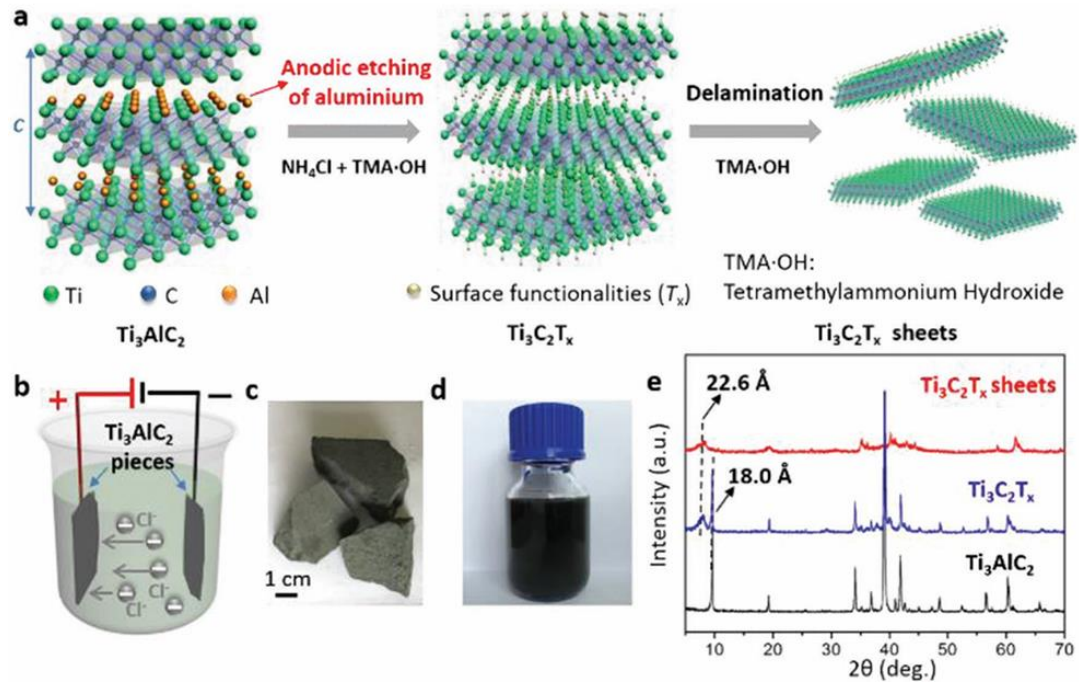


Fig 2. 5 Schematics for electrochemical etching⁶¹

2.3.6 Chemical vapor deposition (CVD)

Xu et al. fabricated “high-quality 2D ultrathin α -Mo₂C crystal with larger-area” in 2015 by CVD. This is another versatile fluoride free etching method where just by altering the relevant CVD growth parameters, transverse dimensions of 2D structure of α -Mo₂C can be altered e.g. high temperature can affect the thickness while lesser temperature changes lateral size. Crystals obtained by this mechanism are much stable under favorable conditions. Superconductivity of ultrathin α -Mo₂C crystals in this experiment was highly reproducible due to better v and thermal stability⁶².

2.4 Properties of MXene

MXene possess unique and diverse structural⁶³, electrochemical, vibrational, transport, mechanical, and magnetic properties⁶⁴. variational surface chemistry, composition and structural chemistry promise energy storage, sensors and nanoscale electronic devices⁶⁵.

2.4.1 Electronic Properties

Electronic properties of MXenes having different functional groups varies in a broad range of properties. A large no of theoretically predicted to little experimentally verified MXenes are found highly conductive metallic²⁹ to half-metallic, semiconducting⁶⁶ to topologically insulating states. Half metallic and topologically insulating MXenes have uniqueness of 100% spin polarization at “Fermi level” and non-trivial edge states are promising for applications of ferromagnetic devices⁶⁷ and valley-spintronics. Variable energy band gap can be achieved using doping⁴⁰, crystal lattice symmetry, stoichiometry engineering⁴⁹, strains⁶⁸ and external electric field to get maximum desirable electronic properties.

A. Lipatov et al. explored higher electrical conductivity of magnitude 10,000S/cm in $Ti_3C_2T_x$ making it a totally novel material⁶⁹. Also metallic to semi-metallic behaviour and tunable bandgap is exhibited using different surface terminations. Higher carrier mobility suitable for field-effect transistor, good electrochemical capacitance due to higher surface area, flexibility and stability under varying environment make MXene much suitable for electrical properties.

2.4.2 Optical properties

Linear and non-linear optical properties are highly dependent on energy band structure of MXene existence of which is already verified. Optical properties in respect of different combinations of of pristine Titanium carbide and nitride are investigated by applying the Random Phase Approximation (RPA) method⁷⁰.

Halim et al reported optical properties of Ti_2CT_x films using Ti_2AlC MAX phase “epitaxial thin films deposited on sapphire substrates” by physical vapor deposition. “Spectroscopic ellipsometry” found in the range of 0.75 to 3.50 eV⁵⁴. Type II band structure is represented by absorption spectra of heterostructures of Mo_2CO_2/W_2CO_2 - in which valence bands and conduction bands are located lower region in comparision to band edges of some another material. This gap allows “confined separation” of electrons and holes in different materials showing blue shift due to charge transfer between different layers⁷¹.

2.4.3 Mechanical properties

MXene show better mechanical properties⁶⁸ than its bulk counterpart. Akinwande et al. 2017 showed value of Young modulus are found better in MXene than graphene and CNTs along with other key features⁶⁸.

Sha et al. 2017 through “1st principle calculations” found 28.5 Giga Pascal (GPa) hardness and 448.9 Giga Pascal (GPa) young modulus concluding Nb₂C-I MXene potentially excellent ultra-stiff material⁷².

2.4.4 Magnetic performance

2D family is enriched as far as magnetic properties are considered. Carbide and nitride of chromium (Cr) and tantalum (Ta) with different n-numbers are expected to be ferromagnets⁷³ with good long range magnetic order that can be extracted from their MAX phases while counterpart of titanium are antiferromagnets.

Hu L et al. conducted computational studies and showed the Mn₂C monolayer is antiferromagnet MXene with Neel temperature=720 K but surface functionalization⁷⁴ like -F, -Cl, and -OH turns it into a ferromagnetic material with higher Curie temperature = 520K⁷⁵. Having said this all, it is a challenge to prepare pristine MXenes like Cr₂C to study magnetic properties, one of the key reasons of comparatively less exploration in this field.

Zhang et al. in year 2019 grew Mo₂C layers on Mo/Cu bilayers substrate by “chemical vapor deposition” giving a typical 2D stacked layers of MXene with lattice defects in the resultant structure. Superconductivity was observed in the defects induced surface by STS 31 technique. Uniform and Strong superconductivity has been observed despite the presence of lattice defects in Mo₂C layer lattice. The transition temperature was almost 8.02K experimentally that was best fitted with theoretical results⁷⁶.

2.5 Transport Properties of MAX and MXene

P. Finkel, et al. has reported the transport properties of ternary transition metal carbide Ti₃SiC₂. Various large grain polycrystalline sample of Ti₃SiC₂ were obtained by sintering, hot

forging after annealing for 24hrs at high temperature of 1600°C. The temperature dependence resistivity measurement of the samples in a field of 5T in temperature regime of 4-300K shows a surprising typical metallic-like behavior at temperature less than 90K. Magnetoresistance (MR) measurements depicts a quadratic dependence upon H, thus revealing this MAX phase is compensated conductor with $n \approx p$ which provides a good agreement with Hall Effect results with high charge carrier concentrations⁷⁷.

Same group extended their study on electronic and transport properties of Ti₃SiC₂, P. Finkel et al. extended their study to its closest member of Ti-Ternary Carbide MAX Phase i.e. Ti₃AlC₂ & Ti₄AlN₃. Their carrier concentration and mobilities, electrical conductivity and magneto-transport properties were studied as a function of temperature in a range from 0K to 300K. Such phase was prepared by mixing Al₄C₃ powders, graphite and titanium at 1400°C for 16hrs at an extreme pressure of 70MPa. Resistivity measurement of Ti₃AlC₂ shows a metallic-like nature down to 80K, and then resistivity drops down linearly with residual resistivity almost 6 times greater than Ti₃SiC₂ thus showing that later former has great defect concentration than later⁷⁷.

A study on electronic, magneto-transport, electrical conductivity, and thermal properties of MAX Phases M₂AlC i.e. M=Ti, V, Nb, Cr in a temperature region of 5K to 300K was investigated by J. D. Hettinger. Again, the results of all these measurement in all of these MAX phases were consistent with two-band model with their electron concentration and mobilities are equal to that of holes. Interestingly, their temperature dependent resistivities measurement shows their metallic-like nature which comes from large density of states close to Fermi level, that is also consistent with the previously studied compounds of the same family⁷⁸.

After comprehensive studies on transport properties of Ti₂AlC and Ti₃AlC₂, Electrical, Hall Effect and transport studies on another member of MAX family Ti₂SiC has been carried out by T. H. Scabarozzi, et al. the resistivity measurements were obtained under 9T as a function of temperature from 2K to 300K. Hot pressing Ti₂SiC powder carried out in vacuum and enveloped in graphite foil placed in a graphite die with heating at 1500°C at 10°C/min for 5hrs. The temperature dependent resistivity measurement shows a metallic like conductivity of the Ti₂SiC down to temperature of ~50K with decreasing effect. Positive and quadratic magnetoresistance effects at all fields and temperature independent negative hall coefficient shows Ti₂SiC is n-type

conductor. All these observations are explained on the basics of Two-band Model upon which most of the MAX Phases are studied⁷⁹.

2.6 Experimental and computational studies on Nb₂C MXene

In 2020 J. Bekaert et al. attempted to unravel superconductivity among MXenes for transition metal elements using “first-principles characterization” along with “Éliashberg formalism”. 3xcarbides MXenes W₂C, Mo₂C, Sc₂C and 3x nitrides Ta₂N, W₂N, Mo₂N. In Mo₂N critical temperature T_c ~16 K is recorded while W₂N reveals the presence of competing superconducting phases⁸⁰.

In 2022 Same group (J. Bekaert et al.) conducted a study “effect of H₂ adatoms to enhance phonon-mediated superconductivity in Nb₂C-MXenes using first-principles calculations in combination with Éliashberg theory” with 3xstructural models hydrogenated Molybdenum and tungsten based MXenes. T_c over 30 K are found for hydrogenated Mo₂N and W₂N revealing different mechanisms involved to enhanced electron–phonon coupling and demonstrated that hydrogen adatoms are reason to induce superconductivity in MXenes that is absent in pristine Nb₂C⁸¹.

In 2022 Kai Wang et al. attempted to resolve the disparity in experimental and computational results of superconducting Nb₂CT_x with different functional groups. They tested superconductivity in Nb₂C MXene using two functional groups like chlorine Cl and Fluorine F making Nb₂CCl_x and Nb₂CF_x. Experiment revealed the “Meissner effect” with zero resistivity for Nb₂CCl_x with T_c ~ 5.2 K while “Ginzburg-Landau parameter κ_{GL}” found to be 2.41 concluding Nb₂CCl_x is a hard superconductor. While, electrical transport and magnetic study analysis proved that Nb₂CF_x is non-superconductor. DFT studies revealed that T_c= 5.2 K for Nb₂CCl_x whereas Nb₂CF_x with imaginary frequency is dynamically unstable that is consistent with the experimental results⁴².

Sheng-Yan et al. in 2022 investigated phonon dispersions, electronic structures and “electron–phonon coupling” of Nb₂CT_x with different terminations like O, Se, S, or Te using first-principles calculations. Results showed that the low energy models for this material are built-in “phonon-mediated” superconductors. Nb₂CO₂ MXene revealed the superconducting critical temperature (T_c) =14.43 K due to contribution of Nb-atoms. Fermi level and soft modes induced

by Kohn anomalies resulted from “strong electron–phonon coupling” ($\lambda=0.92$). Under 4% tensile strain, critical temperature is enhanced reaching upto 18.28K⁸².

The use of MXene in “Electromagnetic interference shielding” was reported in 2016 by Faisal Shahzad and his co-workers. Materials with good flexibility and high conductivity with small thickness are highly required. An EMI shielding of 92 decibels by 45 μ m thick Ti₃C₂T_x film was a successfully achieved which is comparatively higher than other fabricated materials of similar thickness. This comes due to the multiple internal reflections in MXene films and their excellent conductivity (4600 Siemens/cm).

2.7 Superconductivity in MXenes

Impeded research in superconductivity⁸ upsurged after the discovery of 2D materials in recent past⁸³. Xu.C et al. 1st reported superconductivity phenomenon in 2D ultra-thin α -Mo₂C crystal of nanometers thickness with lateral size of 100 μ m acquired using “Chemical Vapor Deposition” (CVD) method at a temperature around 1,085C, a Copper foil placed on a Molybdenum foil acting as a substrate and CH₄ as a carbon source with T_c around 3.6 K. Current vs voltage (IV Curve) measurements in superconducting transition region exhibit power-law dependence on log-log scale in temperature range of 1.8-3.1 K consistent with theoretical model Berezinskii-Kosterlitz-Thouless (BKT) characterization. Before the onset of the superconducting transition, Mo₂C crystal with 8.3 nm thickness shows metallic characteristics measured using Resistance vs Temperature curve ($dR/dT > 0$)⁶².

Baber et al. reported Type-II superconductivity in as-prepared powdered Nb₂C obtained through chemical etching process of bulk Nb₂AlC MAX Phase under optimized condition. Signature for magnetic properties in any sample comes from validation of RT curve, JH curve and Meissner effect. Powdered nature of sample didn’t allow this group to conduct RT measurements to study transport properties while lateral two studies were carried out to get magnetization vs temperature (MT) curve and MH loop for “Zero Field Cooled (ZFC) and Field Cooled (FC)” which confirmed the diamagnetic behaviour of tested sample. Ginzburg-Landau theory was applied for critical fields H_{c1} and H_{c2} to confirm type-II superconductivity. Nb₂C showed the strong “electron-phonon interaction” and the presence of higher density of state at fermi level resulting highest onset transition temperature T_c 12.5 K giving finger prints of Meissner effect⁸⁴.

Where experimental works in the field of superconductivity in MXenes are comparatively less progressive, a good number of density function studies (DFT) are carried out to find out magnetic moment, bonding energy, critical temperature T_c and coherence length.

The gradual efforts done during last ten years to obtain higher T_c for superconductivity in MXene is tabulated below.

Table 2. 1 Transition Temperature T_c for MXene verified experimentally and calculated through DFT Study

MXene	Tc(K)Experimental	Tc (K) DFT study	Year of study	Reference
Mo ₂ C	3.6, 3.48	13 ⁸⁵	2015, 2017	62,86
Mn ₂ N-F ₂	-	1877	2017	87
Mn ₂ N-O ₂	-	1379		
Mn ₂ N-(OH) ₂	-	1743		
Cr ₂ N-O ₂	-	566		
Nb ₂ C	12.5	-	2020	88
Mo ₂ C	-	5.8-7.1	2020	89
Mo ₂ N	-	15.5-16		
W ₂ C	-	5.8-4.2		
W ₂ N	-	9.7-9.8		
Ta ₂ N	-	2.4-2.1		
Sc ₂ C	-	4.0-4.1		
Nb ₂ C	90	-	2024	This work
★This range of T_c varies if Spin-orbit coupling (SOC) is considered or not, respectively.				

2.8 Why Niobium (Nb) MXene?

Niobium is positioned in group 5B of periodic table with atomic no 41 formerly known as Columbium. It is grey(light) refractory transition metal with same ductility as of iron. It oxidizes very slowly in earth's atmosphere. It is commercially used in super alloys and superconductor materials like MRI scanners, nuclear industries, optics, electronics and numismatics. Its most researched superconductor experimentally as well as theoretically.

With its discovery in 2013⁹⁰ niobium with its precursor like Nb₂AlC, Nb₃AlC, Nb₂CT_x attracted more attention due to its promise in different applications like photocatalyst for H₂-evolution, magnetism⁹¹, Li-ion electrodes for battery⁹⁰, photothermal applications³⁴ among others⁵⁴.

Chapter 3: Experimental Synthesis and Introduction to Characterizations

Different methods are used for the synthesis of nano particles. Conversion of a bulk materials to its constituent's particles or the removal of a specific material under controlled circumstances until the required product is formed is named as Top-Down approach. Wet chemical etching and ball milling are very common methods of this approach. Chemical fabrication methods through Top-down are easy to use and have wide range in industrial applications. While, formation of nanostructure from miniaturization of components up to atomic level with the procedure of self-assembly is called as Bottom- Up approach. Any of these two approaches is used as per requirement of the properties and applications required.

3.1 Synthesis Materials and Tools

Chemicals used during synthesis of MXene from its precursor are tabulated below.

Table 3. 1 Chemicals utilized for etching of Nb₂C

Chemicals	Purity	Source
Hydrofluoric acid (HF)	Aldrich 50 wt. % in H ₂ O, ≥99.99%)	Sigma
Niobium Aluminum Carbide Nb ₂ AlC MAX Powder (200 Mesh Size)	95%	
TMAOH (Trimethyl ammonium hydroxide 25% aqueous solution)	25%	
Absolute ethanol	99.8%	Sigma-Aldrich
Acetone	99.8%	Sigma
De-ionized water	99.8%	Sigma

Following materials and tools used in order to obtain the MXene from MAX Phase.

- Digital weight balance
- Teflon Autoclave & Petri dishes
- Hot Plate & Teflon coated Magnetic stirrer

- Vacuum drying Oven
- Vacuum desiccator
 - Safety equipment (goggles, Gas Mask, acid resistant Gloves)
 - Chemical handling apparatus (Spatula, Dropper, Vials, Petri dish, Thermometer)
 - Aluminum foil, butter paper

3.2 Introduction to Characterization Techniques

After synthesis of the MXenes structural, morphological, electrical, electronic and magnetic properties require detailed study using different characterization techniques. Key techniques are listed below.

- X-Ray Diffraction (XRD)
- Scanning Electron Microscopy (SEM)
- Energy dispersive X-Ray Spectroscopy (EDX)
- SQUID (Superconducting Quantum Interface Device, MPMS)
- PPMS (Physical Properties Measuring System)

3.2.1 X-Ray Diffraction (XRD)

X-Ray diffraction is a technique used to identify crystal structure and phase of crystals. It is also used to find out crystallite size using Scherrer formula, lattice parameters and other important terms required to study a material. X-Ray Diffractometer work in accordance to the fundamental principle of optics. When electromagnetic radiations are incident on a plane consist of regular arrangement of obstacles comparable to the wavelength of radiation, diffraction occurs. In solids, there is a regular arrangement of atom, ions and molecules separated by specific interplanar distance in orders of X-Rays wavelength. When X-Ray falls on such atomic lattice, diffraction occurs giving the information about that lattice. This phenomenon is generally used to measure the structure of the material. The diffraction occurring inside crystal is explained by Bragg's law which deals with the diffraction from successive planes of a crystalline structure and provides a fundamental relation between the plane symmetry, incident & diffraction angle and determining the diffraction pattern. As shown in the schematics, the incident X-Ray is diffracted from two consecutive planes, path difference is $2d\sin\theta$ which is the integral

multiple of λ , while d is space between different planes and θ is angle between incident and reflected X-rays.

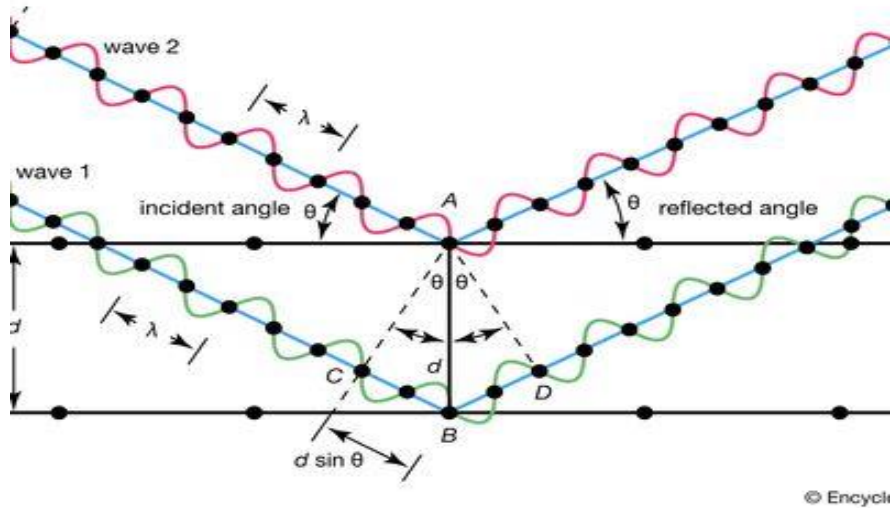


Fig 3. 1 X-Ray diffraction through crystal lattice⁹²

Mathematically;

$$2d\sin\theta = FG + GH$$

$$2d\sin\theta = n\lambda \quad \longrightarrow \quad \text{Braggs Law} \quad (\because FG + GH = n\lambda = \text{path difference})$$

Fundamental principle of this technique is measurement of diffraction intensity as a function of 2θ . The particle size from the diffraction can be calculated using.

$$t = K\lambda A \cos\theta \quad \longrightarrow \quad \text{Sherrer Formula}$$

t = Mean size of the particles

λ = Wavelength of the incident X-rays

K = Dimensional Scherrer constant, typical value is 0.9 A = Line broadening at Full width half maximum

X-Rays are produced by the process of thermionic emission in which high energy electrons produced by heating tungsten filament (copper cathode) are accelerated by high voltage and allowed to fall on a target material (anode). Upon striking the anode, if incident

electrons are suddenly decelerated; X-rays produced are called “baking radiations” or “bremsstrahlung radiations”. When incident electrons have enough energy, inner shells electrons of the target material are knocked out. Such vacancies are filled by upper shells electrons, thus emitting x-rays of energy determined by the electron energy levels.

3.2.2 Scanning Electron Microscopy (SEM)

This technique is used to visualize the topographical surface of the sample by scanning the sample surface with high energy incident electrons. SEM uses electrons that lets us see and detects objects smaller than the wavelength of light itself. Key components of the instrument are shown in schematic diagram. There is an electron gun inside the machine which fires electron. Lenses direct the incident electron on to the target. The bouncing electrons are picked up by the detectors and sent to the monitor that builds up the image.

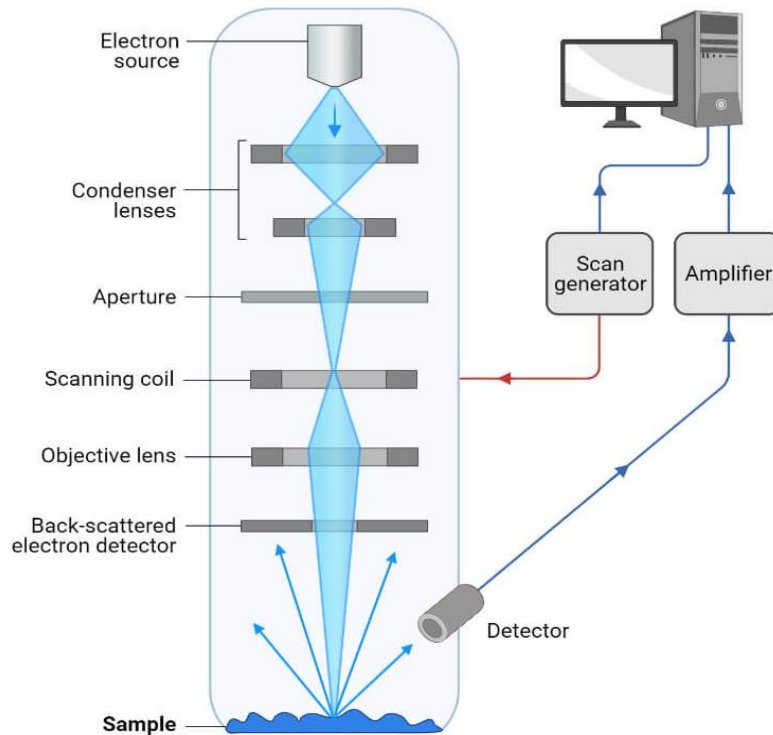


Fig 3. 2 Schematics and working principle of scanning electron microscope⁹³

3.3.3 Energy dispersive X-Ray spectroscopy (EDX)

Energy dispersive X-ray spectroscopy is one of the fundamental techniques to analyze the elemental composition. Every element has different compositions and arrangement of electrons inside the atom. Electrons of an atom reside in specific energy levels having distinct energy difference between them. In SEM, X-rays are produced during interaction of incident beam with sample. Which are used to determine the elemental compositions. The analysis begins as highly energetic incident beam falls on the samples, penetrates deeply inside the samples knocking out the inner shells electrons of the samples. As a result, a vacancy is created which is filled by any electron available in upper shells of the elements atom emitting an X-ray of specific energy. This specific energy corresponds to certain atomic structure. Hence, the sample's elemental composition can be identified with atomic percentage

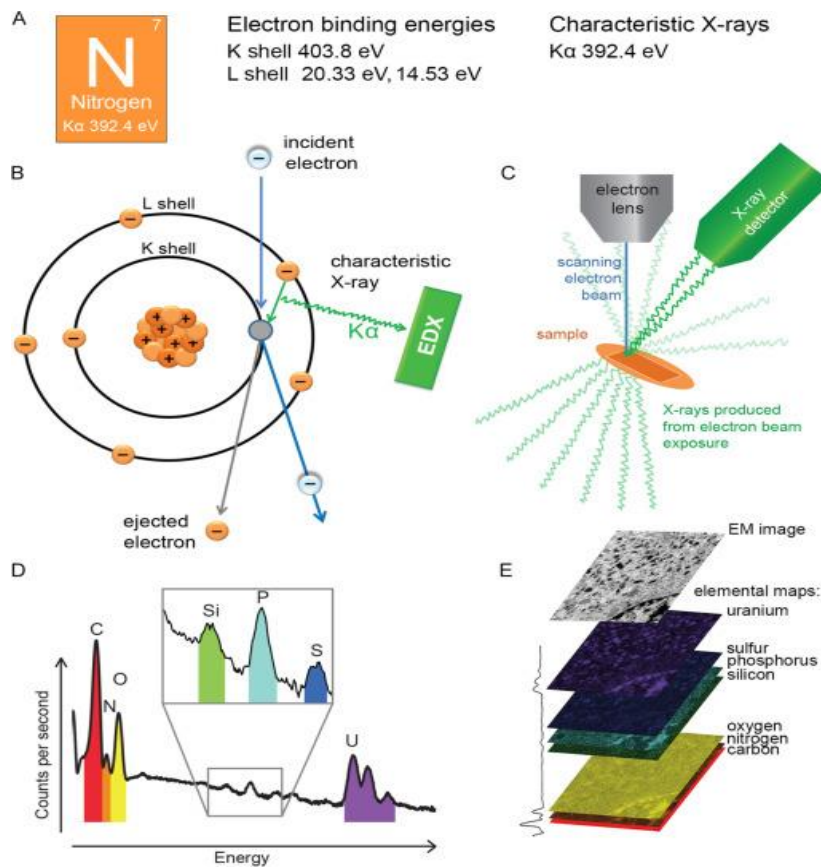


Fig 3. 3 Working principle of energy dispersive X-Ray spectroscopy⁹⁴

3.3.4 SQUID (Superconducting Quantum Interface Device, MPMS)

The magnetic properties measurement involves the magnetic measurements as a function of temperature. It contains “Zero field cooling (ZFC) and Field cooling curves (FC)” and other magnetic measurements as well. In this project, our measurements were performed by using SQUID and PPMS-9 Quantum design. SQUID is the acronym of superconducting quantum interface device operating at cryogenic temperatures with quantum-limited sensitivity. SQUID gives field resolution at the 10^{-17} T level. It consisting of two parallel “Josephson junctions” in which two superconductors are separated by thin insulators. This device has the ability to measure varying magnetic field with the help of these two Josephson Junctions. 2xtypes of SQUIDS include rf-SQUID which has only one Josephson junction that means superconducting ring will be interrupted at single point only while other is DC-SQUID which consist of two Josephson Junctions implies superconducting ring will be interrupted at double points. Devices based upon Josephson have their valuable application in high speed switching circuits. Such devices are manufactured to switch in very small interval of time almost in picoseconds. They also have valuable application in high density computer circuit because of their low dissipation. That is why parallel Josephson junction is used in SQUID to detect very small magnetic fields. In superconductors, the wave function that describes Cooper pairs of electrons is a similar to the wave function of the free particle (exponential like). In the absence of current, all the cooper pairs can be thought of a single wave function with same phase, so can be called a “phase coherent” as by Clarke. As, Josephson junction is made up of two superconducting coils. Cooper pairs experience the process of quantum mechanical tunneling through this insulating layer without breaking their pair. Clarke envisions this tunneling into insulating region, results in interlocking of phase. In results, DC Josephson Effect occurs in which current flow in the absence of applied voltage. To explain working principle of junction consider superconducting magnetic coils producing a magnetic field B through which the sample is moved slowly at a certain frequency with the help of hydraulic system to be safe from mechanical vibrations. Due to this motion, sample magnetic moment induces a change of magnetic flux in these coils. A superconductor loop is formed that transform a part of this flux from coils into the SQUID. Samples must be moved slowly through these pickup coils to remain in safe slewing rate of circuit. (Slewing rate of an electronic circuit

is the rate of change of voltage per unit time). SQUID circuit and input coils have heater that are automatically operated by control module to expel the standing current in the superconducting loops through increasing their temperature above than critical temperature.

3.3.5 Physical Properties Measuring System (PPMS)

Resistivity measurement is the basic measurement through which general and important information about electrical properties of any material can be obtained. The varying resistivity of any sample in comparison to temperature can tells us a lot of information about the nature of the sample and its phase. Especially, performing measurements with magnetic field aids us to explore the materials properties as a function of external field. Generally, four or two probe method is used for resistivity measurements in which voltage drop is calculated through inner probes while passing the current through inner probes. Ohms law is used to measure the resistance as $V=IR$ & $R=V/I$. To study biasing of the sample take Silver or indium pastes are used to make electrical contact in a linear geometry for resistivity measurements as shown in figure. Copper wires are connected with silver paste and placed in a samples holder and its wires are connected to measuring instruments. Moreover, Magnetoresistance measurements i.e. the change in resistance of the sample in the presence of magnetic field are performed. This type of measurements shows significant variation around transition temperatures.

Chapter: 4 Synthesis and Characterization of Nb₂CT_x Free-Standing film

Nb₂CT_x MXene was synthesized using “wet chemical etching method” and subsequently delaminated to obtain free-standing Nb₂CT_x MXene film.

4.1 Synthesis of Nb₂CT_x MXene

In the first step 1g powder of commercially procured MAX Nb₂AlC was etched by gradually mixing it with 10 ml Hydrofluoric acid (48%) following in fume hood. An oil bath was utilized to maintain the 55 °C temperature with continuous uniform magnetic stirring at 400 rpm to make the homogenous solution. After 56 hours the solution from the Teflon line was shifted into a 50 ml centrifuge tube and washed several times at 5000 rpm for 5 mins. In each cycle, the supernatant was discarded and Deionized (DI) water was added various times to the sediment to neutralize the pH of the material and to eliminate the excess HF. Finally, the sediment was filtered through a vacuum assembly and dried at 35 °C in an oven for 24 hours. The obtained MXene was further subjected to the delamination process.

4.2 Synthesis of Nb₂CT_x Free Standing Film

To delaminate Nb₂CT_x MXene the freshly prepared MXene cake was slowly transferred to the solution of 25% TMAOH and Deionized (DI) water. The solution was continuously stirred at 600 rpm for 5 hours similarly using an oil bath to maintain the 55 °C temperature. After 5 hours the solution was centrifuged at 9000 rpm for 5 mins in each cycle to remove the excess TMAOH until the pH became 7. After delamination, the film was obtained by shaking the centrifuge tube for 1 hour by utilizing a vortex and then centrifuge at 3500 rpm to get a few layers of MXene the supernatant was filtered as a multilayer MXene, and the sediment obtained was filtered by using a vacuum assisted assembly which was set for overnight and vacuum oven dried at 55 °C to get single layered MXene film. Systematics for the whole process are shown below in fig 4.1.

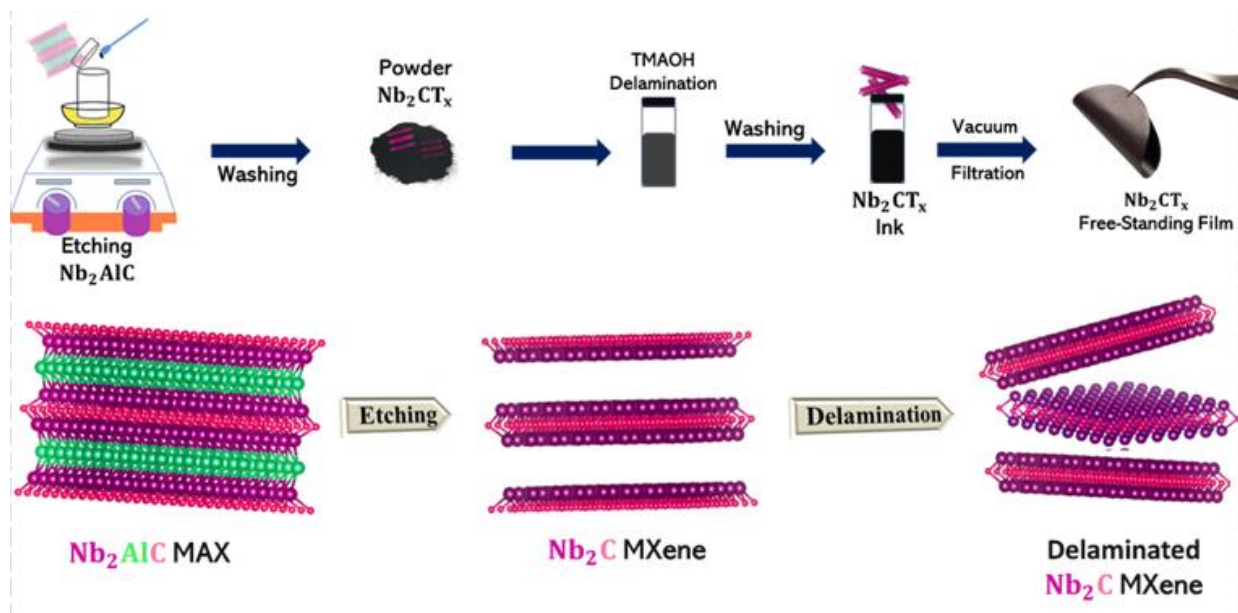


Fig 4. 1 Schematic of synthesis route of Nb_2CT_x free-standing film

4.3 Structural and Morphological Analysis

4.3.1 XRD Analysis

Detailed structural analysis of materials was conducted by utilizing X-ray diffractometry. Fig.4.2(a) demonstrates the XRD spectrum of Nb_2AlC MAX, Nb_2CT_x MXene powder and delaminated Nb_2CT_x MXene film. The peaks of Nb_2AlC MAX were consistent with the earlier reported data JCPDS N: 00-030-0033⁹⁵. After treating the MAX phase with HF by using chemical etching, the peaks of pristine Nb_2CT_x MXene at 8.43° , 33.3° , and 59.5° correspond to (002), (100) and (110) planes respectively. Further the (002) peak at an angle 2-theta 12.7° shifted to a lower angle at 8.43° whereas the decrease in intensity of aluminum peak at 38.1° corresponded to the plane (103) indicating the successful exfoliation of Nb_2CT_x MXene similarly there is the little amount of unetched Nb_2AlC MAX was treated unreacted. As a result, the c-lattice parameter increased from 13.92 to 20.3, the enhancement in the c-lattice parameter might be due to the elimination of aluminum from the MAX phase. After etching prepared Nb_2CT_x MXene powder resulted in delamination to get a free-standing film of Nb_2CT_x MXene in which enhanced lattice parameters along the c-axis were observed.

Furthermore, the c-Lp of Nb₂CT_x MXene to a free-standing film of Nb₂CT_x MXene raised from 20.3 to 28.24. Fig 4.2(b) shows the comparison of d spacing and c-Lp of MAX phase, MXene and free-standing film.

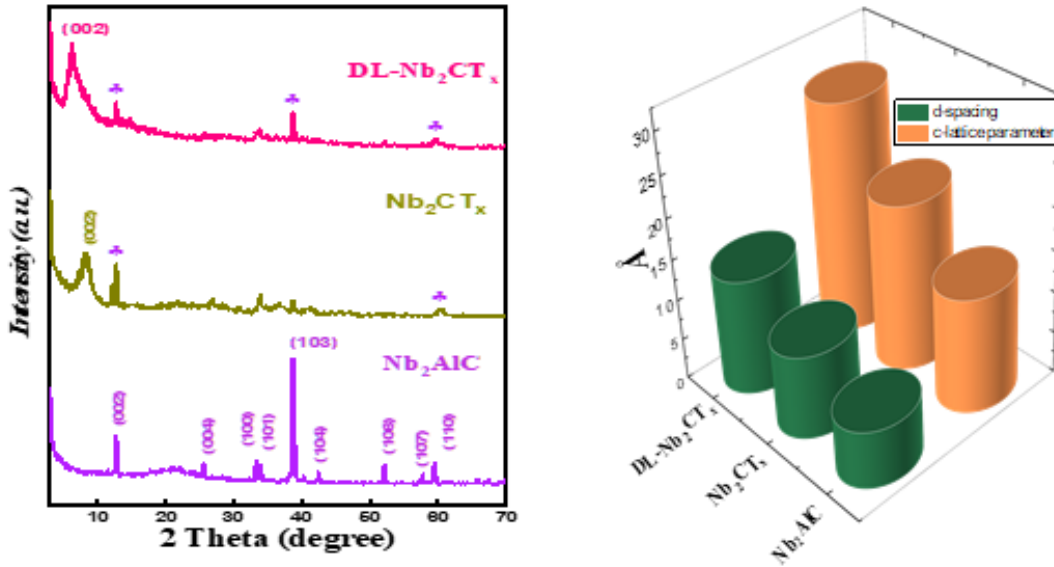


Fig 4. 2 (a) XRD spectra of the MAX Nb₂AlC, Nb₂CT_x MXene and Nb₂CT_x MXene Free-standing film

(b) comparison plot of d-spacing and c-lattice parameter of each material.

4.3.2 SEM & EDX Analysis

A “scanning electron microscopy” (SEM) was carried out to view the magnified image of Nb₂AlC MAX, Nb₂CT_x MXene powder and delaminated Nb₂CT_x MXene film as displayed in Fig. 4.3(a-c) whereas the elemental composition of each element was analyzed by employing “energy-dispersive X-ray spectroscopy” (EDX) as shown in Fig. 4.3(d) The surface morphology of Nb₂AlC MAX phase showing the ceramic particle structure as illustrated in Fig. 4.3(a) whereas after etching the opening of MXene sheets can be seen on Fig. 4.3(b) which also confirms the formation of layered 2D MXene structure. Fig. 4.3(c) shows the image of a delaminated Nb₂CT_x MXene indicating an uneven arrangement of MXene flakes and successful delamination of Nb₂CT_x MXene film. Fig. 4.3(d) shows the atomic and weight percent of Nb₂CT_x MXene displaying the composition of each element similarly the terminations (F, O) attached to it also was observed. From Nb₂AlC MAX (S1) to Nb₂CT_x MXene the atomic % of oxygen is increased from 11.6 to 18.4 % while the

atomic % of fluorine has also been found to be 2 % due to the exfoliation by utilizing hydrofluoric acid (HF).

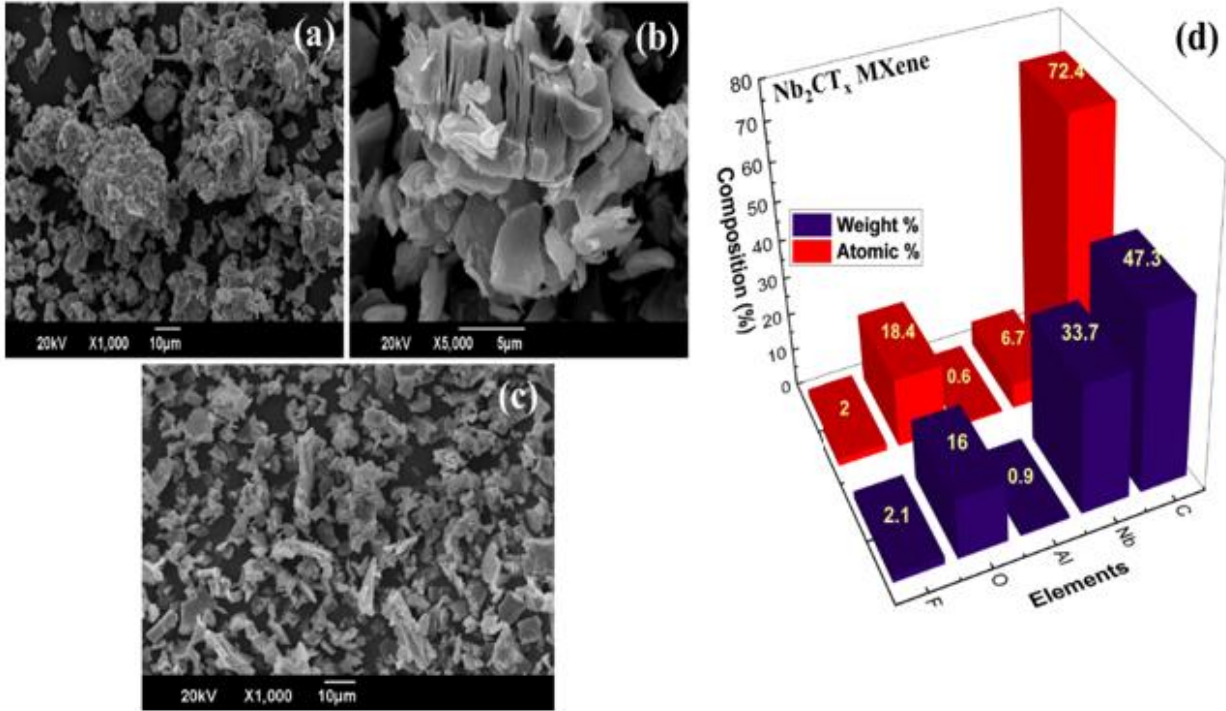


Fig 4. 3 SEM images of (a) Nb₂AlC MAX phase at 10 μm (b) HF etched Nb₂CT_x MXene at 5 μm (c) Delaminated Nb₂CT_x MXene at 10 μm (d) Elemental analysis of each element in Nb₂CT_x MXene Free-standing film.

4.3.3 XPS Studies

“X-ray Photoelectron spectroscopy” (XPS) was used to get the chemical composition and bonding of as-prepared Nb₂CT_x MXene. Fig. 4.4(a) exhibits the presence of all main elements (Nb, C, O, F) present in Nb₂CT_x MXene. Fig. 4.4(b-d) shows the deconvoluted high-resolution XPS spectrum of different element regions. High Resolution XPS Spectra of the Nb₂CT_x MXene in the Nb 3d region reveal three peaks at 203.2, 206.2, and 209.1 eV as illustrated in Fig. 4.4(b). The peak at 203.2 eV (3d_{5/2}) belongs to Nb-C bonding⁹⁶ whereas the peaks at 206.2 (3d_{5/2}) and 209.1 eV (3d_{3/2}) represent the bonding of Nb-O and Nb₂-O₅⁹⁷ respectively. Furthermore, the C 1s region shows three major peaks at

281.4, 284.0 and 286.3 eV as demonstrated in Fig. 4.4(c). The peaks at 281.4, 284.0 and 286.3 eV are attributed to Nb-C, C-C and C-O bonding respectively⁹⁸. The termination attached to MXene after the HF treatment was also confirmed by the XPS plot as shown in Fig. 4.4d. Similarly, the peaks at 529.5 and 531.2 eV in O 1s spectrum are consistent with bonds Nb-O and Nb-C-O respectively^{97,99}. The XPS spectra confirm the successful preparation of our prepared Nb₂CT_x MXene.

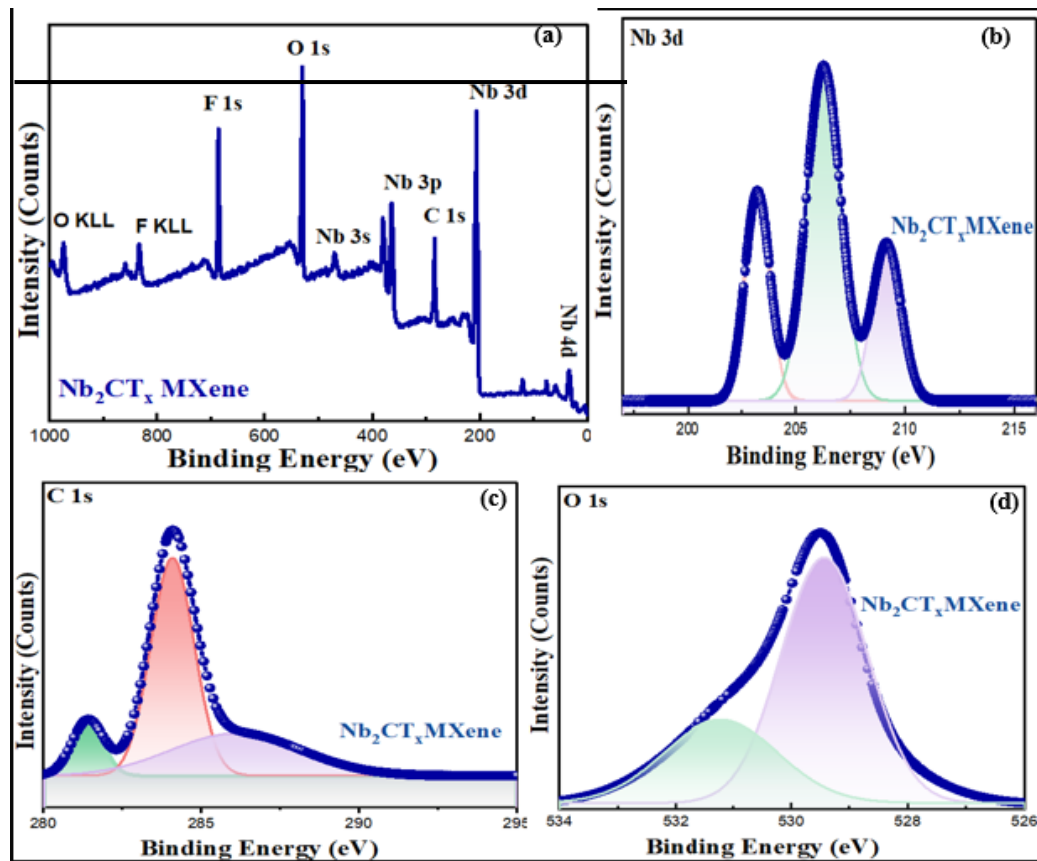


Fig 4. 4 . (a) XPS spectra for Nb₂CT_x MXene. Deconvolution of high-resolution XPS plot for Nb₂CT_x MXene (b) Nb 3d (c) C 1s (d) O 1s

Chapter: 5 Magneto-Transport properties of Nb₂CT_x Free-Standing Film

Superconductivity in free standing film of Nb₂C is investigated employing superconducting quantum interface device (SQUID) Magnetometer MPMS3. Temperature vs magnetization and temperature vs resistivity (RT) curves are obtained for study.

5.1 Temperature dependent magnetization

For our sample Nb₂CT_x free-standing film, Fig. 5.1(a) represents ZFC curve indicating negative value of magnetic moment that confirms diamagnetic nature of Nb₂C. The signature for superconductivity is splitting of curves obtained for temperature vs magnetization (MT) at all temperatures under a range of external magnetic fields from 50 Oe to 1k Oe (Supporting Info 2). Baber *et al.* in 2020 studied Nb₂AlC-MAX and Nb₂C MXene pointing out paramagnetic and diamagnetic (with magnetic moment of -0.00485 μ_B) natures respectively using DFT study¹⁰⁰. A phase transition at T_c=87K is present in free standing film exhibiting proximity effect. Fig. 5.1(b-d) shows MT field cooled (FC) curves obtained under an applied field of 50 Oe, 100 Oe, 500 Oe and 1k Oe where magnetization curves depict an increase in phase transition temperature T_c=90K against its previously found values of 12.5K in powdered form attributed to the confinement of magnetic flux resulting from the flux pinning. We further notice an increment of 3K in transition temperature for FC curve in comparison to ZFC curve arising due to application of magnetic field which causes enhanced electron-phonon coupling (EPC) due to low dimensionality and confinement effect irrespective of field strength. There is a gradual decrease in magnetization upon decrease in temperature attributed to vortex formation below T_c. Also, higher strengths of applied magnetic field shows shifting of curves towards paramagnetic behavior in Nb₂C possibly due to the existence of counter magnetic phases. Presence of competing phases studied by M. Iqbal *et al.* in un-doped and La-doped Ti₃C₂T_x MXene synthesized using “co-precipitation method” indicated the co-existence of ferromagnetic-antiferromagnetic phases in 2D carbides¹⁰¹. The vortices at low temperature are stationary and magnetic flux pinning among them become stronger, showing strong superconductivity, while further increase in temperature destroys flux pinning among the layers of film thus bringing material back to normal state/ paramagnetic state from superconducting state at temperature higher than T_c. Density function theory (DFT) studies carried out by Baber *et al.* in 2020 conclude that pristine MXene Nb₂C exhibits unconventional superconductor like behavior irrespective of functional group termination⁸⁴ while same study by

Wang K *et al.* in 2022 point out the possible reason for superconductivity in Nb₂C is the presence of O₂ as functional group⁴². Keeping in view our ZFC and FC curves, intrinsic diamagnetic property argument for Nb₂C seems more convincing.

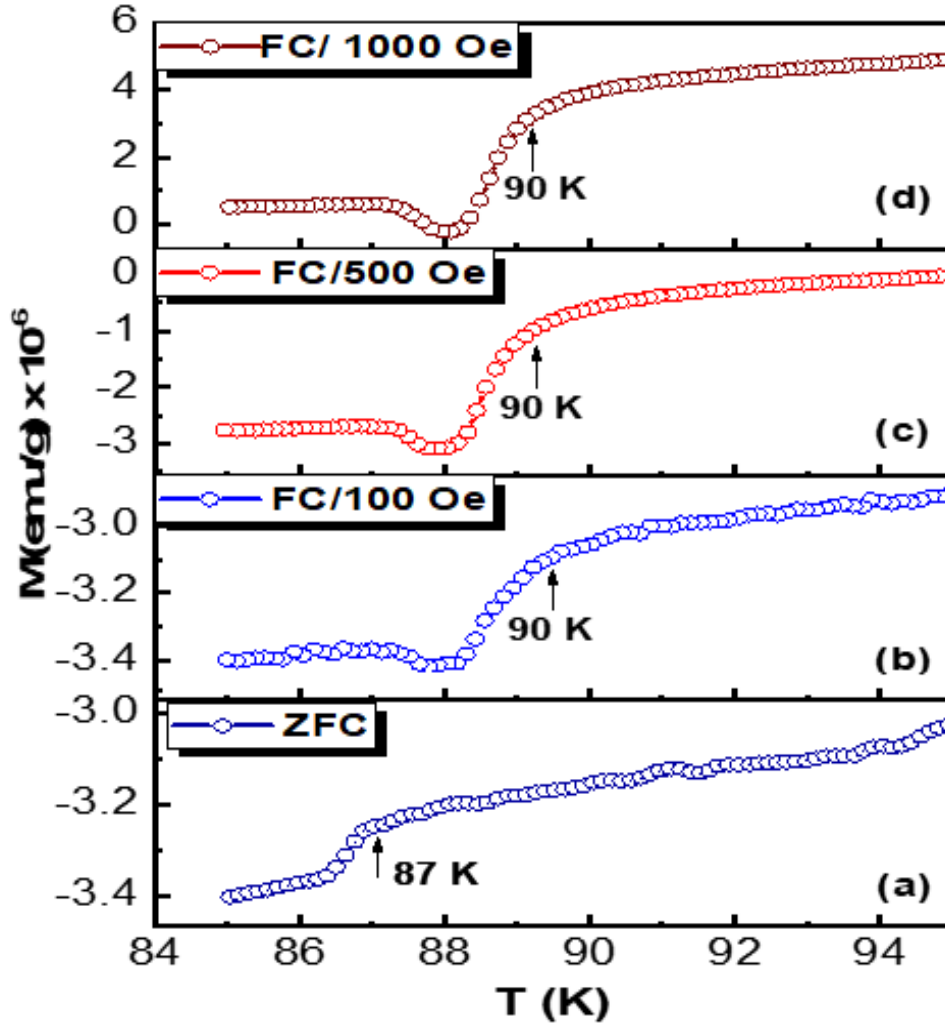


Fig 5. 1 ZFC and FC curves at 100 Oe, 500 Oe and 1K Oe for Nb₂C free-standing film

5.2 Magneto-transport Properties

Fig. 5.2(a) shows temperature vs resistivity (left Y-axis) and Temperature vs magnetic moment (right Y-axis) at H=0 for Nb₂C free standing film. MT-curve shows a transition at T_M=87K with a sharp positive gradient whereas resistivity shows transition at T_ρ=82K. Both curves show transition approximately at the same point with a slight lag of 5K by ρT-curve likely due to

different external factors arise during film formation process like any variation of temperature during whole process, moisture, cleaning conditions⁶⁵ or may be due to functional group modelling during etching. ρT -curve is trending towards superconducting phase which terminates at 51.8K here while extrapolating towards negative temperature zone same trend confirms superconductor Nb₂C free standing film while left thread of MT-curve indicates more negative trend of magnetic moment exhibiting diamagnetic nature of our sample, fact already established via magnetization curves in this paper.

Fig. 5.2(b) ρT -curve under FC at 50 Oe and 100 Oe reveals transition point (T_c) at 84.6K and 58K respectively forming two temperature zones. i.e. Higher temperature zone where $T > T_c$ and lower temperature zone with $T < T_c$. For **region $T > T_c$** resistance increase with decrease in temperature with negative gradient consistent with weak localization effect a feature that exist in low dimension materials¹⁰². Same has been elucidated by Babr *et al.* for Nb₂C mechanically pressed pellet with prominent semiconductor behaviour⁹¹. For $T < T_c$ inclination toward superconductor behaviour is present under different magnetic fields while at 1k Oe increased para-magnetism killed superconductivity at critical point of 129K. Here, two attributes are discernible: Suppression of superconducting phase at lower temperatures at higher applied fields and negligible magnetoresistance in the normal state¹⁰³. Two mechanisms are present to investigate this dichotomy i.e. Orbital effect that is coupling between external field and electron momentum and spin paramagnetic effect in which cooper pair, as the core of BCS theory are formed at cryogenic temperature (less than McMillan limit), spin gets aligned with external magnetic field⁸³. For low dimensions orbital affect can be neglected while later seems responsible of this transition. Low temperature zone, increase in external magnetic field increases paramagnetic behaviour killing diamagnetic superconductivity due to the formation of anti-vortices. Xu, X. *et al.* recently reported wafer-scale MXene thin film fabricated implying an anisotropic diamagnetic superconductivity¹⁰⁴ in Nb₂C MXene attributed towards Berezinskii-Kosterlitz-Thouless (BKT) transition. Our result also shows binding and unbinding of vortex-antivortex pairs forming superconductor state and normal state respectively. This may happen due to increased magnetic field. Under T greater than T_c indicate unbinding of vortex pairs showing dominance of quantum effect and BKT characterization. It further depicts the existence of critical value of external field H_c in the range greater than 50 Oe but less than 100Oe for superconducting phase.

Summarily, in the presence of magnetic field Type-II superconductor Nb₂C carry large transport current in lesser temperature zone with dominant superconductor behaviour whereas in higher temperature zone with higher external fields superconductivity diminishes consistent with BKT properties.

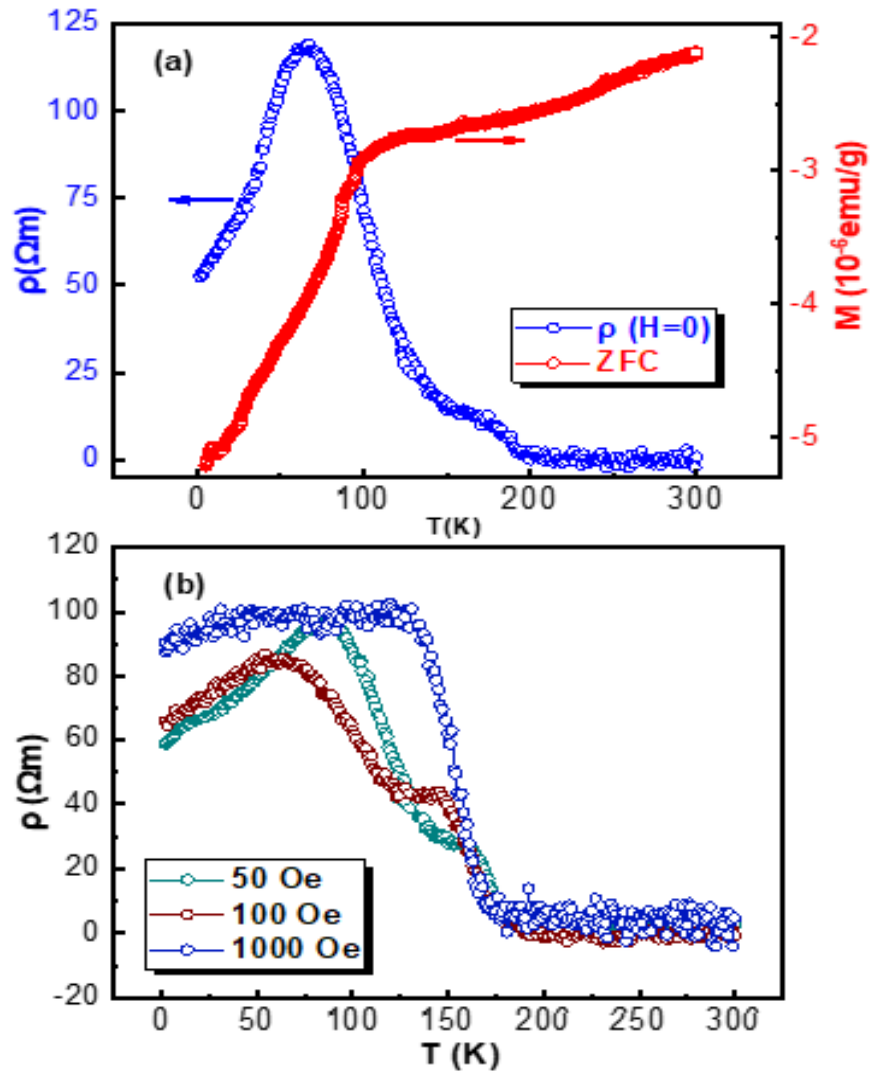


Fig 5. 2 (a) Temperature vs Resistivity (left y-axis) and magnetic moment (right Y-axis) at $H=0$,

(b) Temperature vs resistivity at 50 Oe, 100 Oe and 1k Oe

Conclusion

Summarily, I have successful prepared Nb_2CT_x MXene free-standing film by etching of Nb_2AlC MAX phase after establishing optimization conditions. MAX powder was immersed into Hydrofluoric acid (48%) at $55\text{ }^\circ\text{C}$ temperature for 56hours. Delamination was done after etching following standard procedure. Characterization tests confirmed successful etching where lattice parameters showed significant peak shift in flakes. SEM images confirm lamellar structure and EDX confirms element composition of free-standing film. Chemical bonding is studied using XPS. Temperature dependent magnetization confirms diamagnetic type-II superconductivity as intrinsic nature of Nb_2C with transition temperature $T_c = 90\text{K}$ under field cooled applied magnetic field of 50 Oe, 100 Oe and 500 Oe. Such high “ T_c ” can be attributed to strong electron-phonon coupling and high density of state (DOS) near fermi level. Proximity effect and confinement of magnetic flux resulting from the flux pinning in free standing film seems main cause for this much higher transition temperature. Magneto-transport properties studied using temperature-resistance curve showed flow of large amount of current under threshold applied field around 50 Oe. Shift from diamagnetic towards paramagnetic behaviour due to anti-vortex formation is noticed. Previous work on same material was limited due to powdered form of the sample. Transport studies in this work are in novel and connected with work already done.

Increased superconductivity with much higher T_c and critical magnetic field gives a way forward to more practically attainable spintronics.

Future Perspective

My study on MXene, particularly in the fields of magnetism described in this dissertation will serve as a roadmap for scholars to go further into the growing field of 2D materials especially in the field of magnetism and superconductivity in MXene.

HF etching has its own hazards so development of safe and efficient green etching techniques for A layer removal at room temperature is important concern and requires alternative findings.

DFT studies provide a clear hint of existence of superconductivity in nitride-based MXene. Study requires experimental verification to fully harness the potential of this family.

References

1. Gogotsi, Y. The Future of MXenes. *Chemistry of Materials* vol. 35 8767–8770 Preprint at <https://doi.org/10.1021/acs.chemmater.3c02491> (2023).
2. Novoselov, K. S. Nobel Lecture: Graphene: Materials in the Flatland. *Rev Mod Phys* **83**, 837–849 (2011).
3. Gogotsi, Y. & Anasori, B. The Rise of MXenes. *ACS Nano* vol. 13 8491–8494 Preprint at <https://doi.org/10.1021/acsnano.9b06394> (2019).
4. Bhat, A. *et al.* Prospects challenges and stability of 2D MXenes for clean energy conversion and storage applications. *npj 2D Materials and Applications* vol. 5 Preprint at <https://doi.org/10.1038/s41699-021-00239-8> (2021).
5. Gibertini, M., Koperski, M., Morpurgo, A. F. & Novoselov, K. S. *Magnetic 2D Materials and Heterostructures*.
6. Ghosh, K., Rahaman, H. & Bhattacharyya, P. Prediction and Implementation of Graphene and Other Two-Dimensional Material Based Superconductors: A Review. *IEEE Transactions on Applied Superconductivity* **30**, (2020).
7. http://www.zswu.dicp.ac.cn/Research/Synthesis___Assembly_Chemistry_of_2D_Materials.htm.
8. Devices, N., Liou, J. J., Liaw, S.-K. & Chung, Y.-H. Also of Interest. in *Zeitschrift für Naturforschung A. A Journal of Physical Sciences* (2017).
9. Matthias, B. T. & Hulm, J. K. *A Search for New Superconducting Compounds*.
10. Willens, R. H., Buehler, E. & Matthias, B. T. *Superconductivity of the Transition-Metal Carbides*. vol. 159 (1967).
11. *Handbook of Superconductivity*.
12. <https://en.wikipedia.org/wiki/Superconductivity>.
13. Mazin, I. I. Superconductivity gets an iron boost. *Nature* vol. 464 183–186 Preprint at <https://doi.org/10.1038/nature08914> (2010).
14. Bussmann-Holder, A. & Keller, H. High-temperature superconductors: Underlying physics and applications. *Zeitschrift für Naturforschung - Section B Journal of Chemical Sciences* 3–14 (2019) doi:10.1515/znb-2019-0103.
15. Drozdov, A. P., Erements, M. I., Troyan, I. A., Ksenofontov, V. & Shylin, S. I. Conventional superconductivity at 203 kelvin at high pressures in the sulfur hydride system. *Nature* **525**, 73–76 (2015).

16. Zhou, T. *Mechanism of High Temperature Superconductivity-the BCS Theory and a New Electron Pairing Medium*.
17. Maksimov, E. G. High-temperature superconductivity: the current state. *Physics-Uspekhi* **43**, 965–990 (2000).
18. Zhou, T. *Mechanism of High Temperature Superconductivity-the BCS Theory and a New Electron Pairing Medium*.
19. https://en.wikipedia.org/wiki/Meissner_effect.
20. Qing, J., Haixia, C. & Zhenya -, L. *Ordering, Metastability and Phase Transitions in Two-Dimensional Systems You May Also like Gauge Equivalent Structures of the Integrable (2+1)-Dimensional Nonlocal Nonlinear Schrödinger Equations and Their Applications Xiaoming Zhu-The Spin Correlation Functions of a Semi-Infinite Heisenberg Ferromagnet M G Cottam-Critical Properties of Anisotropic Heisenberg Ferromagnet with Spin-One. J. Phys. C: Solid State Phys* vol. 6 (1973).
21. Flores-Livas, J. A. *et al.* A perspective on conventional high-temperature superconductors at high pressure: Methods and materials. *Physics Reports* vol. 856 1–78 Preprint at <https://doi.org/10.1016/j.physrep.2020.02.003> (2020).
22. Kechik, M. M. A. *Effect of Yb2O3 Nanoparticle Addition on Superconducting Properties of BSCCO (2223)/Ag Tapes by Acetate Precipitation Method Article in Pertanika. Journal of Science and Technology* vol. 2 <https://www.researchgate.net/publication/308983900> (2016).
23. <https://cse.umn.edu/irm/2-classes-magnetic-materials>.
24. Billah, A. Investigation of multiferroic and photocatalytic properties of Li doped BiFeO₃ nanoparticles prepared by ultrasonication. (2016) doi:10.13140/RG.2.2.23988.76166.
25. <https://en.wikipedia.org/wiki/Antiferromagnetism>.
26. <https://sciencenotes.org/paramagnetic-vs-diamagnetic-vs-ferromagnetic-magnetism/>.
27. <https://en.wikipedia.org/wiki/Nanotechnology>.
28. Choi, W. *et al.* Recent development of two-dimensional transition metal dichalcogenides and their applications. *Materials Today* vol. 20 116–130 Preprint at <https://doi.org/10.1016/j.mattod.2016.10.002> (2017).
29. Naguib, M. *et al.* Two-dimensional nanocrystals produced by exfoliation of Ti₃AlC₂. *Advanced Materials* **23**, 4248–4253 (2011).
30. Anasori, B. *et al.* Two-Dimensional, Ordered, Double Transition Metals Carbides (MXenes). *ACS Nano* **9**, 9507–9516 (2015).

31. Novel synthesis methods and applications of MXene-based nanomaterials.
32. Verger, L. *et al.* Overview of the synthesis of MXenes and other ultrathin 2D transition metal carbides and nitrides. *Current Opinion in Solid State and Materials Science* vol. 23 149–163 Preprint at <https://doi.org/10.1016/j.cossms.2019.02.001> (2019).
33. Novel synthesis methods and applications of MXene-based nanomaterials.
34. Griffith, K. J. *et al.* Bulk and Surface Chemistry of the Niobium MAX and MXene Phases from Multinuclear Solid-State NMR Spectroscopy. *J Am Chem Soc* **142**, 18924–18935 (2020).
35. Li, G. *et al.* Epitaxial growth and physical properties of 2D materials beyond graphene: From monatomic materials to binary compounds. *Chemical Society Reviews* vol. 47 6073–6100 Preprint at <https://doi.org/10.1039/c8cs00286j> (2018).
36. Naguib, M. *et al.* Two-dimensional transition metal carbides. *ACS Nano* **6**, 1322–1331 (2012).
37. Halim, J. *et al.* Electronic and optical characterization of 2D Ti₂C and Nb₂C (MXene) thin films. *Journal of Physics Condensed Matter* **31**, (2019).
38. Hart, J. L. *et al.* Control of MXenes' electronic properties through termination and intercalation. *Nat Commun* **10**, (2019).
39. Akinwande, D. *et al.* A review on mechanics and mechanical properties of 2D materials—Graphene and beyond. *Extreme Mechanics Letters* vol. 13 42–77 Preprint at <https://doi.org/10.1016/j.eml.2017.01.008> (2017).
40. Hakim, M. W. *et al.* Ni-intercalated Mo₂TiC₂T_x free-standing MXene for excellent gravimetric capacitance prepared via electrostatic self-assembly. *J Energy Storage* **61**, (2023).
41. Ahmad, S., Ashraf, I., Mansoor, M. A., Rizwan, S. & Iqbal, M. An overview of recent advances in the synthesis and applications of the transition metal carbide nanomaterials. *Nanomaterials* vol. 11 1–36 Preprint at <https://doi.org/10.3390/nano11030776> (2021).
42. Wang, K. *et al.* Role of surface functional groups to superconductivity in Nb₂C-MXene: Experiments and density functional theory calculations. *Surfaces and Interfaces* **29**, (2022).
43. Sun, Z., Music, D., Ahuja, R., Li, S. & Schneider, J. M. Bonding and classification of nanolayered ternary carbides. *Phys Rev B Condens Matter Mater Phys* **70**, (2004).

44. Naguib, M., Mochalin, V. N., Barsoum, M. W. & Gogotsi, Y. 25th anniversary article: MXenes: A new family of two-dimensional materials. *Advanced Materials* **26**, 992–1005 (2014).
45. Shuck, C. E. *et al.* Safe Synthesis of MAX and MXene: Guidelines to Reduce Risk during Synthesis. *ACS Chemical Health and Safety* **28**, 326–338 (2021).
46. Och, M., Martin, M. B., Dlubak, B., Seneor, P. & Mattevi, C. Synthesis of emerging 2D layered magnetic materials. *Nanoscale* vol. 13 2157–2180 Preprint at <https://doi.org/10.1039/d0nr07867k> (2021).
47. Zhou, C. *et al.* A review of etching methods of MXene and applications of MXene conductive hydrogels. *European Polymer Journal* vol. 167 Preprint at <https://doi.org/10.1016/j.eurpolymj.2022.111063> (2022).
48. Tang, M. *et al.* Surface Terminations of MXene: Synthesis, Characterization, and Properties. *Symmetry* vol. 14 Preprint at <https://doi.org/10.3390/sym14112232> (2022).
49. Srivastava, P., Mishra, A., Mizuseki, H., Lee, K. R. & Singh, A. K. Mechanistic Insight into the Chemical Exfoliation and Functionalization of Ti₃C₂ MXene. *ACS Appl Mater Interfaces* **8**, 24256–24264 (2016).
50. Lipatov, A. *et al.* Effect of Synthesis on Quality, Electronic Properties and Environmental Stability of Individual Monolayer Ti₃C₂ MXene Flakes. *Adv Electron Mater* **2**, (2016).
51. Ghidui, M., Lukatskaya, M. R., Zhao, M. Q., Gogotsi, Y. & Barsoum, M. W. Conductive two-dimensional titanium carbide ‘clay’ with high volumetric capacitance. *Nature* **516**, 78–81 (2015).
52. Zhu, Y. *et al.* Multifunctional Ti₃C₂T_xMXene Composite Hydrogels with Strain Sensitivity toward Absorption-Dominated Electromagnetic-Interference Shielding. *ACS Nano* **15**, 1465–1474 (2021).
53. Liu, F. *et al.* Preparation of High-Purity V₂C MXene and Electrochemical Properties as Li-Ion Batteries. *J Electrochem Soc* **164**, A709–A713 (2017).
54. Halim, J. *et al.* Electronic and optical characterization of 2D Ti₂C and Nb₂C (MXene) thin films. *Journal of Physics Condensed Matter* **31**, (2019).
55. Halim, J. *et al.* Transparent conductive two-dimensional titanium carbide epitaxial thin films. *Chemistry of Materials* **26**, 2374–2381 (2014).
56. Feng, A., Yu, Y., Mi, L., Yu, Y. & Song, L. Comparative study on electrosorptive behavior of NH₄HF₂-etched Ti₃C₂ and HF-etched Ti₃C₂ for capacitive deionization. *Ionics (Kiel)* **25**, 727–735 (2019).

57. Natu, V. *et al.* 2D Ti₃C₂T_z MXene Synthesized by Water-free Etching of Ti₃AlC₂ in Polar Organic Solvents. *Chem* **6**, 616–630 (2020).
58. Urbankowski, P. *et al.* Synthesis of two-dimensional titanium nitride Ti₄N₃ (MXene). *Nanoscale* **8**, 11385–11391 (2016).
59. Sun, W. *et al.* Electrochemical etching of Ti₂AlC to Ti₂CT:X (MXene) in low-concentration hydrochloric acid solution. *J Mater Chem A Mater* **5**, 21663–21668 (2017).
60. Yang, S. *et al.* Fluoride-Free Synthesis of Two-Dimensional Titanium Carbide (MXene) Using A Binary Aqueous System. *Angewandte Chemie - International Edition* **57**, 15491–15495 (2018).
61. Yu, H. *et al.* Surface Modified MXene-Based Nanocomposites for Electrochemical Energy Conversion and Storage. *Small* vol. 15 Preprint at <https://doi.org/10.1002/sml.201901503> (2019).
62. Xu, C. *et al.* Large-area high-quality 2D ultrathin Mo₂C superconducting crystals. *Nat Mater* **14**, 1135–1141 (2015).
63. Khazaei, M., Arai, M., Sasaki, T., Estili, M. & Sakka, Y. Trends in electronic structures and structural properties of MAX phases: A first-principles study on M₂AlC (M = Sc, Ti, Cr, Zr, Nb, Mo, Hf, or Ta), M₂AlN, and hypothetical M₂AlB phases. *Journal of Physics Condensed Matter* **26**, (2014).
64. Champagne, A. & Charlier, J. C. Physical properties of 2D MXenes: From a theoretical perspective. *JPhys Materials* vol. 3 Preprint at <https://doi.org/10.1088/2515-7639/ab97ee> (2020).
65. Zhang, L. *et al.* Influencing Factors on Synthesis and Properties of MXene: A Review. *Processes* vol. 10 Preprint at <https://doi.org/10.3390/pr10091744> (2022).
66. Khazaei, M. *et al.* Novel electronic and magnetic properties of two-dimensional transition metal carbides and nitrides. *Adv Funct Mater* **23**, 2185–2192 (2013).
67. Tahir, R., Zahra, S. A., Naeem, U., Akinwande, D. & Rizwan, S. First observation on emergence of strong room-temperature ferroelectricity and multiferroicity in 2D-Ti₃C₂T_x free-standing MXene film. *RSC Adv* **12**, 24571–24578 (2022).
68. Akinwande, D. *et al.* A review on mechanics and mechanical properties of 2D materials—Graphene and beyond. *Extreme Mechanics Letters* vol. 13 42–77 Preprint at <https://doi.org/10.1016/j.eml.2017.01.008> (2017).
69. Lipatov, A. *et al.* High electrical conductivity and breakdown current density of individual monolayer Ti₃C₂T_x MXene flakes. *Matter* **4**, 1413–1427 (2021).
70. Gao, L. *et al.* Optical Properties of Few-Layer Ti₃CN MXene: From Experimental Observations to Theoretical Calculations. *ACS Nano* **16**, 3059–3069 (2022).

71. Modi, N. *et al.* Theoretical investigations of asymmetric functionalized Y2C-based MXene monolayers. *Solid State Commun* **372**, (2023).
72. Sha, X., Xiao, N., Guan, Y. & Yi, X. Structural, mechanical and electronic properties of Nb2C: First-principles calculations. *RSC Adv* **7**, 33402–33407 (2017).
73. Zhang, Y. & Li, F. Robust half-metallic ferromagnetism in Cr3C2 MXene. *J Magn Mater* **433**, 222–226 (2017).
74. Jiang, X. *et al.* Two-dimensional MXenes: From morphological to optical, electric, and magnetic properties and applications. *Physics Reports* vol. 848 1–58 Preprint at <https://doi.org/10.1016/j.physrep.2019.12.006> (2020).
75. Hu, L., Wu, X. & Yang, J. Mn2C monolayer: A 2D antiferromagnetic metal with high Néel temperature and large spin-orbit coupling. *Nanoscale* **8**, 12939–12945 (2016).
76. Zhang, Z. *et al.* Layer-Stacking, Defects, and Robust Superconductivity on the Mo-Terminated Surface of Ultrathin Mo 2 C Flakes Grown by CVD. *Nano Lett* **19**, 3327–3335 (2019).
77. Finkel, P., Barsoum, M. W., Hettinger, J. D., Lofland, S. E. & Yoo, H. I. Low-temperature transport properties of nanolaminates Ti3AlC2 and Ti4AlN3. *Phys Rev B Condens Matter Mater Phys* **67**, (2003).
78. Hettinger, J. D. *et al.* Electrical transport, thermal transport, and elastic properties of M2AlC (M=Ti, Cr, Nb, and V). *Phys Rev B Condens Matter Mater Phys* **72**, (2005).
79. Scabarozzi, T. H. *et al.* Electrical, thermal, and elastic properties of the MAX-phase Ti2 SC. *J Appl Phys* **104**, (2008).
80. Bekaert, J., Sevik, C. & Milošević, M. V. *First-Principles Exploration of Superconductivity in MXenes* *First-Principles Exploration of Superconductivity in MXenes* †.
81. Bekaert, J., Sevik, C. & Milosevic, M. V. Enhancing superconductivity in MXenes through hydrogenation. (2022).
82. Wang, S. Y. *et al.* Straintronic Effect on Phonon-Mediated Superconductivity of Nb2CT2(T = O, S, Se, or Te) MXenes. *Journal of Physical Chemistry C* **126**, 3727–3735 (2022).
83. Qiu, D. *et al.* Recent Advances in 2D Superconductors. *Advanced Materials* vol. 33 Preprint at <https://doi.org/10.1002/adma.202006124> (2021).
84. Babar, Z. U. D. *et al.* Peculiar magnetic behaviour and Meissner effect in two-dimensional layered Nb2C MXene. *2d Mater* **7**, (2020).

85. Lei, J., Kutana, A. & Yakobson, B. I. Predicting stable phase monolayer Mo₂C (MXene), a superconductor with chemically-tunable critical temperature. *J Mater Chem C Mater* **5**, 3438–3444 (2017).
86. Song, S. *et al.* Magnetotransport in Ultrathin 2-D Superconducting Mo₂C Crystals. *IEEE Trans Magn* **53**, (2017).
87. Kumar, H. *et al.* Tunable Magnetism and Transport Properties in Nitride MXenes. *ACS Nano* **11**, 7648–7655 (2017).
88. Felner, I. Peculiar magnetic features and superconductivity in sulfur doped amorphous carbon. *Magnetochemistry* vol. 2 Preprint at <https://doi.org/10.3390/magnetochemistry2030034> (2016).
89. Bekaert, J., Sevik, C. & Milošević, M. V. First-principles exploration of superconductivity in MXenes. *Nanoscale* **12**, 17354–17361 (2020).
90. Naguib, M. *et al.* New two-dimensional niobium and vanadium carbides as promising materials for li-ion batteries. *J Am Chem Soc* **135**, 15966–15969 (2013).
91. Babar, Z. U. D., Zheng, R. K., Mumtaz, M. & Rizwan, S. Magneto-transport of mechanically-pressed niobium carbide (Nb₂C) distorted MXene. *Mater Lett* **285**, (2021).
92. <https://www.britannica.com/science/Bragg-law>.
93. <https://microbenotes.com/scanning-electron-microscope-sem/>.
94. <https://www.sciencedirect.com/topics/agricultural-and-biological-sciences/energy-dispersive-x-ray-analysis>.
95. Ali, I., Zahra, S. A., Sajid, I. H. & Rizwan, S. Efficient electrochemical performance of electrostatically self-assembled Nb₂CTx/AgNPs-CTAB nanocomposite in both basic and neutral electrolytes. *J Energy Storage* **88**, (2024).
96. Teixeira Da Silva, V. L. S., Schmal, M. & Oyama, S. T. Niobium Carbide Synthesis from Niobium Oxide: Study of the Synthesis Conditions, Kinetics, and Solid-State Transformation Mechanism. *J Solid State Chem* **123**, 168–182 (1996).
97. Halim, J. *et al.* X-ray photoelectron spectroscopy of select multi-layered transition metal carbides (MXenes). *Appl Surf Sci* **362**, 406–417 (2016).
98. Dong, H. *et al.* Molten Salt Derived Nb₂CTx MXene Anode for Li-ion Batteries. *ChemElectroChem* **8**, 957–962 (2021).
99. Li, Y. *et al.* A general Lewis acidic etching route for preparing MXenes with enhanced electrochemical performance in non-aqueous electrolyte. *Nature Materials* **2020 19:8 19**, 894–899 (2020).

100. Din Babar, Z. U. *et al.* Magnetic phase transition from paramagnetic in Nb₂AlC-MAX to superconductivity-like diamagnetic in Nb₂C-MXene: An experimental and computational analysis. *RSC Adv* **10**, 25669–25678 (2020).
101. Iqbal, M. *et al.* Co-existence of magnetic phases in two-dimensional MXene. *Mater Today Chem* **16**, (2020).
102. Bergmann, G. *WEAK LOCALIZATION IN THIN FILMS a Time-of-Flight Experiment with Conduction Electrons. Review Section of Physics Letters* vol. 107 (1984).
103. Hu, R., Lauritch-Kullas, K., O'Brian, J., Mitrovic, V. F. & Petrovic, C. Anisotropy of electrical transport and superconductivity in metal chains of Nb₂Se₃. *Phys Rev B Condens Matter Mater Phys* **75**, (2007).
104. Xu, X. *et al.* Anisotropic Superconducting Nb₂CT_x MXene Processed by Atomic Exchange at the Wafer Scale. *Advanced Materials* **36**, (2024).